Operational platform for metocean forecasts in Thermaikos Gulf (Aegean Sea, Greece)

Yannis Androulidakis, Christos Makris, Vassilis Kolovoyiannis, Katerina Kombiadou, Yannis Krestenitis, Stergios Kartsios, Ioannis Pytharoulis, Vasilis Baltikas & Zisis Mallios

Taylor & Francis
Taylor & Francis Group

Check for updates

Operational platform for metocean forecasts in Thermaikos Gulf (Aegean Sea, Greece)

Yannis Androulidakis[a,b], Christos Makris[a,c], Vassilis Kolovoyiannis[b], Katerina Kombiadou[a,d], Yannis Krestenitis[a], Stergios Kartsios[e], Ioannis Pytharoulis[e], Vasilis Baltikas[a] and Zisis Mallios[a]

[a]Division of Hydraulics and Environmental Engineering, School of Civil Engineering, Aristotle University of Thessaloniki, Thessaloniki, Greece; [b]Laboratory of Physical and Chemical Oceanography, Department of Marine Sciences, University of the Aegean, Mytilene, Greece; [c]Sector of Hydraulics and Environmental Engineering, Department of Civil Engineering, Democritus University of Thrace, Xanthi, Greece; [d]Centre for Marine and Environmental Research (CIMA) / Aquatic Research Network (ARNET), University of Algarve, Faro, Portugal; [e]Department of Meteorology and Climatology, School of Geology, Aristotle University of Thessaloniki, Thessaloniki, Greece

ABSTRACT

Thermaikos Gulf, located in the northeastern Mediterranean Sea, faces significant anthropogenic pressures and natural hazards, requiring reliable metocean forecasts for weather, ocean circulation, sea levels, waves, and hazard predictions, including pollutant transport, coastal floods, and freshwater discharges. The Wave4Us operational platform addresses these needs by providing high-resolution and specialised forecasts, accessible to local authorities, researchers, and the public. Additionally, on-demand predictions for marine pollution, coastal inundation, and heatwaves offer real-time insights to emergency responders and coastal authorities during hazardous events. This study presents the platform's structure, modelling advancements, and predictive skill for specific hazards. Forecast efficiency is evaluated against satellite and field observations: (i) the simulated oil spill spreading is verified by satellite data; (ii) the modelled freshwater discharges are validated against field measurements (high correlation, RMSE < 10%); (iii) a pronounced river plume spreading is confirmed by ocean/tracer simulations and satellite imagery; (iv) the prediction of sea level, wave conditions, and coastal flooding under a severe low-pressure system is validated against measurements and documented events; (v) the marine heatwave predictions is confirmed by comparing simulated and satellite sea temperatures (error < 1%). These evaluations demonstrate the platform's reliability in forecasting key environmental risks, aiding decision-making and response efforts in the Thermaikos Gulf region.

1. Introduction

Thermaikos Gulf (TG) is a naturally protected and partially enclosed embayment in the north-western Aegean Sea (Figure 1a), with two rather narrow entrances in its northern part. It is influenced by various anthropogenic stressors and natural factors. The littoral zone of TG is approximately 250 km long, expanding from its northernmost point near the coastal city of Thessaloniki (1.1 million residents) and down to its southernmost boundary with the open sea, at Kassandra Peninsula (Figure 1a). The most important freshwater inputs are provided by a system of two large (Axios and Aliakmonas) and two small rivers (Gallikos and Loudias), an intermittent river (Anthemountas), several ephemeral streams, and a network of farming drainage channels (e.g. Milovou and Chalastra), located mainly along the western coastal zone (Figure 1b; Karageorgis et al. 2005). These freshwater sources are crucial for the hydrology and ecology of the gulf, influencing its

seawater quality, nutrient levels, benthic health, and ecosystem dynamics (Kaberi et al. 2023; Androulidakis et al. 2024a), as well as the stratification, circulation and renewal of the gulf (Krestenitis et al. 2012; Androulidakis et al. 2023a). Agricultural and aquacultural activities are scattered along the western areas, whereas urban, industrial, and touristic zones are primarily concentrated in the northern and eastern regions of the gulf. Maritime traffic and port operations are additional pressures to the marine environment, especially over the northern parts of the gulf. The environmental vulnerability of the TG is linked to several factors such as eutrophication events (Genitsaris et al. 2019), frequent hydrocarbon releases (Zafirakou 2019), marine plastic pollution (e.g. Tzioga and Moriki 2023), chronic coastal erosion areas (Kombiadou and Krestenitis 2012), flooding over low-lying areas (Figure 1c; Androulidakis et al. 2023c), fisheries' overexploitation (Dimarchopoulou et al. 2024), hazardous weather events (Pytharoulis et al. 2016; Pytharoulis et al. 2021), and intense Marine
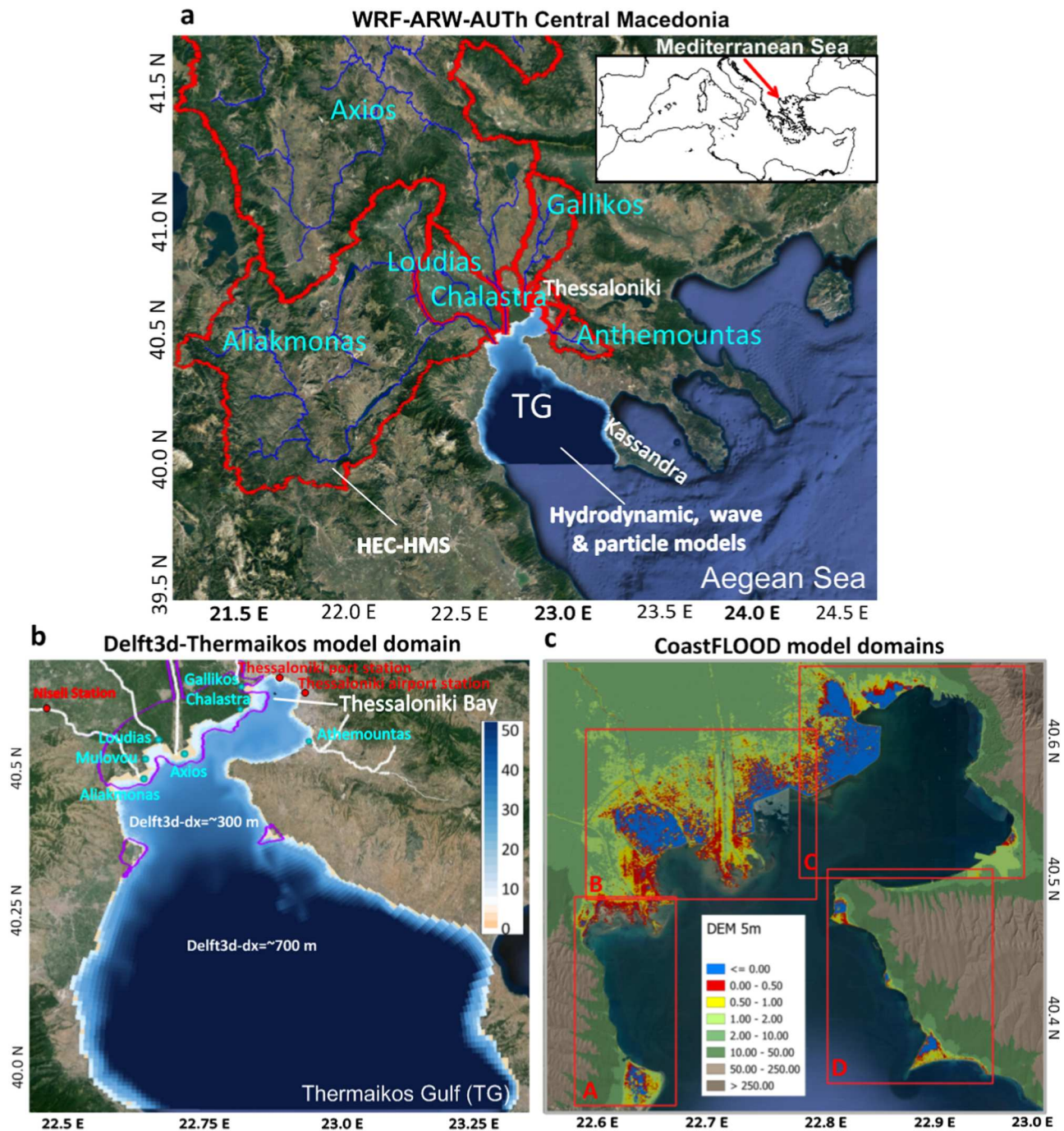
Figure 1. (a) Domains of the WRF-ARW-AUTh model, HEC-HMS model (red lines: drainage basins; blue lines: river network). The insert Mediterranean map marks the location of Thermaikos Gulf (TG). (b) Bathymetry (m) of the Delft3D-Thermaikos model grid with river-mouth freshwater point sources (light blue fonts), Thessaloniki Bay, NATURA 2000 areas (purple hatches), Niseli station at Aliakmonas river, Thessaloniki airport station (meteorological), Thessaloniki port station (tide-gauge). (v) Domains (red squares) of the CoastFLOOD model over a 5 m Digital Elevation Model (DEM) background; colour scale represents land elevation in metres.

Heatwaves (MHWs; Androulidakis and Krestenitis 2022). The water quality in the TG degraded significantly during the 1970s and 1980s, mainly due to population increase and the complete absence of urban and industrial wastewater treatment (Androulidakis et al. 2024a). While a trend of gradual improvement has been observed

since the 1990s, the desired objective of achieving a 'good environmental state', as mandated by national legislation and EU directives, has yet to be fully accomplished, despite the high percentage of population (88% in 2015; Prochaska and Zouboulis 2020) connected to tertiary Wastewater Treatment Plants (WTP).

The high socioenvironmental importance of TG stems primarily from: (a) the densely populated coastal zone and accompanying infrastructure and (b) the existence of important wetlands and protected areas, predominantly located along its western coasts, with large river deltas and NATURA 2000 areas (Figure 1b; Kaberi et al. 2023). However, after reviewing the relevant scientific literature, Androulidakis et al. (2024a) documented a decline in field monitoring initiatives of the TG during the last decade; the decline was drastic enough to currently classify TG in the data-poor areas in terms of field observations. TG is also a coastal system of particular interest towards the digital transformation, advocated by the EU strategic priorities until 2030 (European Commission 2023). Consequently, daily high-resolution short-term predictions of prevailing environmental conditions, such as weather patterns and marine characteristics, is of paramount importance and necessity (Androulidakis et al. 2024a), especially in the absence of a consistent and reliable monitoring network. As health and safety levels are profoundly influenced by the state and quality of the marine environment, particularly within the context of climate change, these types of forecasts, along with targeted mid- and long-term simulations considering climate scenarios, can offer valuable insights to relevant stakeholders, including authorities, professionals, the scientific community, and, of course, the citizens residing in coastal areas.

Large-scale regional forecasting platforms for atmospheric and ocean predictions that cover the TG, are available by the Copernicus Marine Service (2024) for the Mediterranean Sea (CMS; Coppini et al. 2023) and from other operational platforms for regional seas, such as the POSEIDON System (2024), operating in the Aegean Sea (Korres et al. 2002) and the Aegean-Levantine Forecast System (ALERMO 2024; Skliris et al. 2007). However, their spatial resolution is low and cannot support operational products over the TG and other densely populated coastal areas along the Mediterranean coast. This gave rise to the development of several high-resolution early warning systems, such as the Balearic Islands Coastal Observing and Forecasting System (SOCIB 2024; Juza et al. 2016; Sotillo et al. 2021), the Hydro-Meteo-Climate Service of the Agency for Prevention, Environment and Energy of Emilia-Romagna (Arpae-SIMC; Biolchi et al. 2021), the Sistema de Apoyo Meteorológico y Oceanográfico de la Autoridad Portuaria for the ports of Spain (SAMOA 2024; Sotillo et al. 2020; García-León et al. 2022), the Accu-Waves platform for major Mediterranean ports (Makris et al. 2021; Makris et al. 2024a), the high-resolution COASTAL Forecasting system for the island of Crete (COASTAL CRETE 2024; Spanoudaki et al. 2021), the Cyprus Coastal Ocean Forecasting System (CYCOFOS 2024; Zodiatis et al. 2003), the South Eastern Levantine Israeli Prediction System (SELIPS 2024; Tintoré et al. 2019), the Coastal Environmental Observatory for Northern Aegean (AEGIS 2024; Zervakis et al. 2023), and the Wave4Us (http://wave4us.web.auth.gr) forecasting platform in the TG (Krestenitis et al. 2014). Wave4Us is developed and maintained by the Laboratory of Maritime Engineering and Maritime Works (LMEMW) of the Aristotle University of Thessaloniki (AUTh; Greece) and was initially set to provide daily forecasts of sea level, ocean circulation, wave and weather conditions (Krestenitis et al. 2015). The system has evolved since, with improvements to modelling approaches, integration of freshwater influx and additional operational and on-demand forecast products, tailored to the vulnerabilities of the system to natural and anthropogenic hazards. The performance of some of the modelling components of the platform's integrated forecast suite has been evaluated using both field and satellite observations (Pytharoulis et al. 2015a; Pytharoulis et al. 2015b; Krestenitis et al. 2017; Androulidakis et al. 2021; Makris et al. 2021; Pytharoulis et al. 2021; Androulidakis et al. 2023a; Makris et al. 2023a; Androulidakis et al. 2023b; Androulidakis et al. 2023c).

Here, we describe the structure and capabilities of the Wave4Us operational platform, in terms of specific model components, integration and data flow, allowing for the replicability of the approach in similar systems. In its present form, Wave4Us is a forecasting platform that presents various novelties, as it offers: (a) very high spatial detail and high level of model integration, necessary to account for all major forcing factors and physical processes; (b) unique prognoses of freshwater influence to the thermohaline stratification and circulation of the Gulf; (c) targeted, on-demand, products to assist key stakeholders in mitigating marine and coastal hazardous events (marine pollution, coastal flooding or maritime accidents). Aside from elaborating on the approach, the present study aims to identify the main strengths and weaknesses of the system by assessing model skill for specific and characteristic examples of recent extreme events in the TG, as well as to highlight important and characteristics processes that are often overlooked in similar systems. Additionally, the set of provided model applications is based on the specific needs of local stakeholders (e.g. protection against marine pollution and coastal flooding), which are not accommodated by other operational platforms.

Section 2 describes the main components of Wave4Us, focusing on recently incorporated elements

of the platform for specialised forecasting products. In Section 3, we showcase the operational system's performance in simulating specific natural and human-related hazardous events. Section 4 summarises conclusions and discusses future steps.

2. Methodology

The Wave4Us platform covers several processes that affect the marine environment and the coastal zone of the TG, addressed with meteorological, hydrological, hydrodynamic, wave, particle-tracking, and coastal flooding simulations. The model grids cover different regions of the study area, with a broader domain for the atmospheric and hydrological models (Figure 1a), the TG domain for hydrodynamic, wave, and particle-tracking models (Figure 1b), and the finer resolution domains for the coastal flooding model over the northern TG (Figure 1c). The main modules of the modelling platform, the respective predicted parameter fields, and the coupling scheme for the system's components are presented in Figure 2. The operational modules of the platform (meteorology, hydrology, circulation, storm surges and waves) have varying degrees of coupling, depending on the modelled processes and the related

main forcing factors (Figure 2). Wave4Us provides 3-day forecasts, updated daily at 08:30 UTC, with products uploaded on the Wave4Us website as spatial distributions and time-series and/or cross-sections in areas of interest (selectable through the 'Results type selection' drop-down menu). On-demand services, such as tracers of pollutants due to accidents (e.g. oil spills) and connectivity pathways to assist search-and-rescue actions, are also provided after direct (e-mail or telephone) requests to LMEMW. The main attributes of the system's modelling components are described below.

2.1. Meteorological forecasts

High-resolution forecasts of the meteorological conditions are conducted with the Weather Research and Forecasting model with the Advanced Research dynamic solver (WRF-ARW; Wang et al. 2014) by the Laboratory of Meteorology and Climatology of AUTh (WRF-ARW-AUTh 2024; Pytharoulis et al. 2015a, 2015b). The integrated weather forecast system, with a 96-hour forecasting horizon, relies on three one-way nested meteorological simulations over three domains of gradually decreasing coverage and
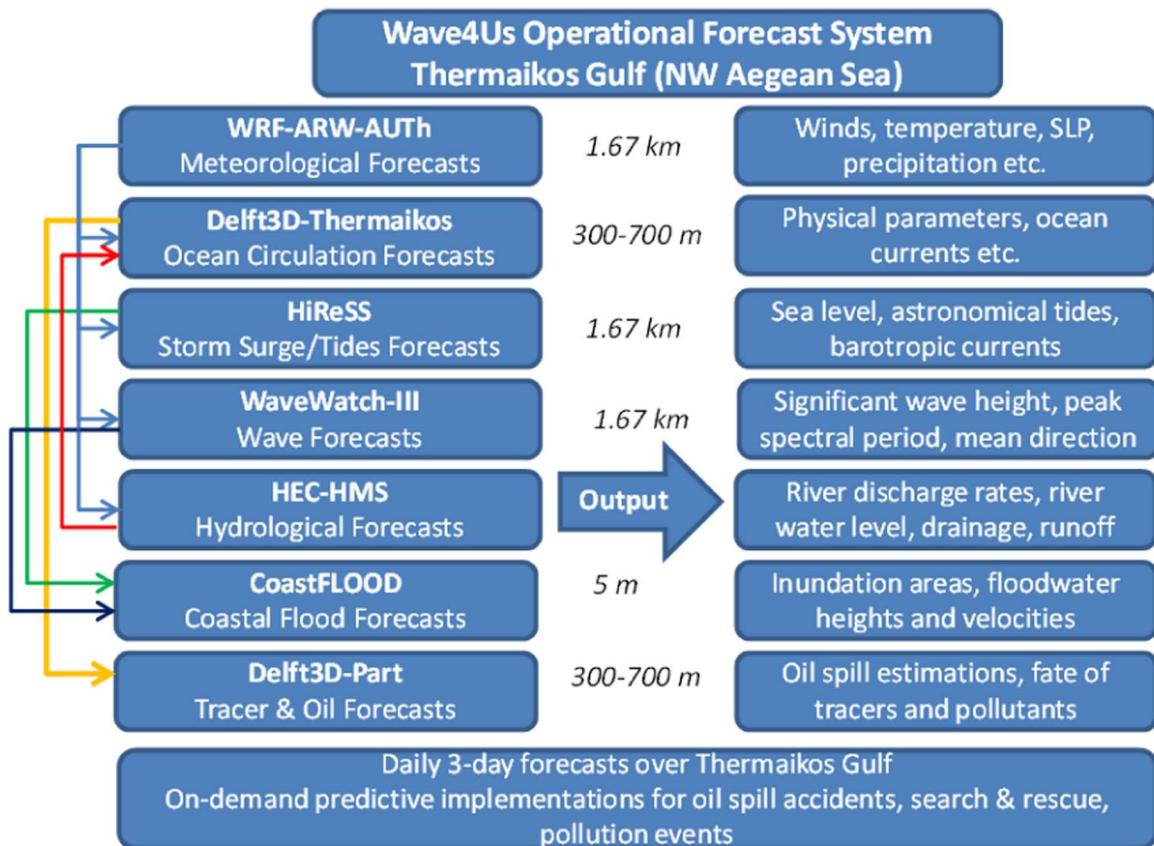
Figure 2. Wave4Us operational platform (modules, interactions, coupling schematics, model resolution, and featured output).

increasing resolution: (i) over the European continent (15 km × 15 km grid; domain d01), (ii) over the central and eastern Mediterranean (including Apennine and Balkan peninsulas; 5 km × 5 km grid; domain d02), and, (iii) the wider Central Macedonia region (1.67 km × 1.67 km grid; domain d03; Figure 3). The marine area of interest (TG) is integrated at the high horizontal domain d03 (Figure 1a) that represents the complex physiographic characteristics of Central Macedonia. The boundary conditions for d03 are provided by the forecasts of domain d02. All three domains employ thirty-nine sigma levels (up to 50 hPa) with higher vertical resolution near the surface. The produced hourly atmospheric datasets consist of wind velocities, sea level pressure, air temperature, relative humidity, cloudiness, surface heat fluxes, and precipitation fields. The meteorological model is initialised daily at 12:00 UTC of the previous day, using the global analysis of the Global Forecasting System (GFS) of the National Center for Environmental Prediction (NCEP) with a grid spacing of 0.25° × 0.25°. The global forecasts of GFS are used for boundary conditions of the outer domain (domain d01) of WRF-ARW-AUTh. The GFS global analyses/forecasts are widely used by numerous international modelling groups as initial/boundary conditions for the operational production of numerical weather predictions, due to their quality, resolution and uninterrupted availability without any cost. The Sea Surface Temperature (SST) values are based on the daily global dataset of NCEP (of the day before the model initialisation) with a grid spacing of 1/12° × 1/12°. In terms of process parameterisation, WRF-ARW-AUTh uses the following schemes: Ferrier (Rogers et al. 2001) for microphysics, Betts-Miller-Janjić (Janjić 1994) for cumulus convection in the two outer domains, RRTMG (rapid radiative transfer model application for global climate models; Iacono et al. 2008) for radiation, Mellor-Yamada-Janjić (Mellor and Yamada 1982; Janić 2002) for the boundary layer, Monin-Obukhov (Eta; Janjić 1994) for the surface layer and the NOAH (NCEP/Oregon State University/Air Force/Hydrologic Research Lab) Unified model (Chen and Dudhia 2001) for soil processes (in 4 layers down to 2 m below land surface). The daily meteorological forecasts for all domains are freely available on the website (WRF METEO AUTH) of the Department of Meteorology and Climatology of AUTh. The WRF-ARW-AUTh modelling system setup has been validated for large periods, various synoptic conditions, and extreme events (Pytharoulis et al. 2015a; Pytharoulis et al. 2015b; Krestenitis et al. 2017; Pytharoulis et al. 2021; Androulidakis et al.

2023c). The output of the 12–96 forecast hours (i.e. 3.5 days ahead) are used to force the hydrologic, hydrodynamic, and wave simulations (Figure 2).

2.2. Hydrological forecasts

Riverine freshwater influx to the TG is a critical factor for stratification and circulation in the gulf (Krestenitis et al. 2012). To account for these influences, the daily discharge rates at the freshwater sources around the TG are provided by the Hydrologic Modeling System (HEC-HMS 2024; Androulidakis et al. 2021), associated to the respective drainage basins over the Central Macedonia (Frysali et al. 2023; Figure 1a). The main freshwater input of the TG comes from four perennial rivers (Gallikos, Axios, Loudias, and Aliakmonas; Figure 1b), with lower and occasional outflows by the Anthemountas intermittent river (Figure 1b) and by the complex network of streams, torrents, irrigation canals, and trench drains of the area (e.g. Chalastra sub-basin; Figure 1a). The main stem of the Aliakmonas River is completely controlled by the dams built along its course, with a cascade of five large dams that are used for power generation and to cover the needs for irrigation and water supply of the wider region. HEC-HMS simulates the complete hydrologic processes of the entire dendritic watershed systems, including many traditional procedures of hydrologic analysis, such as event infiltration, unit hydrographs, and hydrologic routing. To account for even the smallest freshwater inflows to the TG, HEC-HMS was integrated into the Wave4Us system not only for major rivers, but also for the intermittent and ephemeral stream networks (Figure 1b). The freshwater inflows from the six main sources discharging into the basin, used as input for the circulation forecasts (see Section 2.3), were parameterised based on the following:

- Evapotranspiration: Meteorological data for precipitation and atmospheric temperature (from WRF-ARW-AUTh).
- Digital Elevation Map: EEA-10 (2024) by the Copernicus platform.
- Basic Land Cover data: Corine Land Cover 2018.
- Other Land Cover data: Pan-European High-Resolution Layers about imperviousness, forests, grasslands, water bodies & wetness, small woody features by the Copernicus platform (CLMS 2024).
- Soil Data: 3-D Soil Hydraulic Database of Europe (European Soil Data Centre 2024).
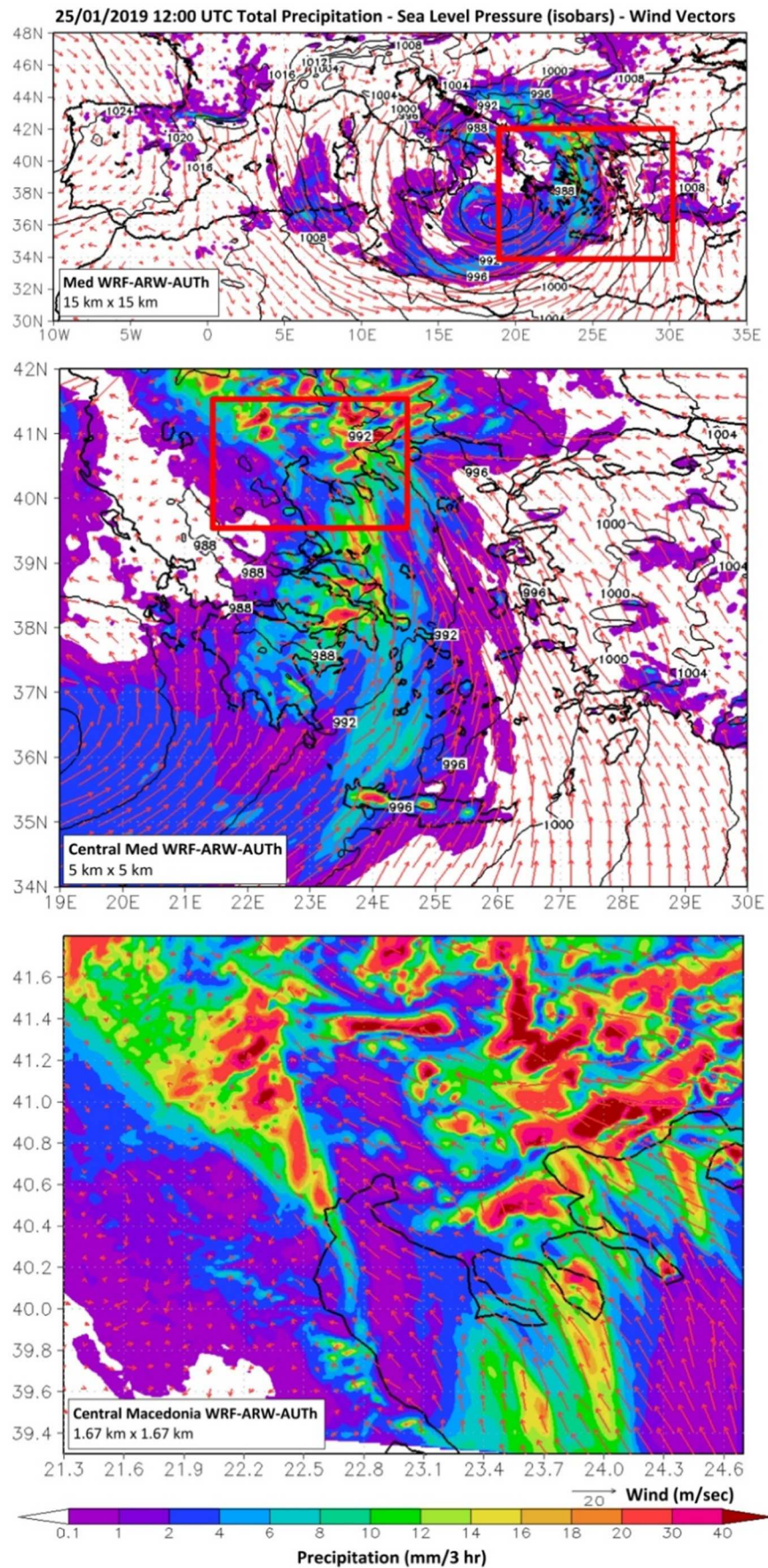
Figure 3. Map of meteorological variables (precipitation: coloured contours, mean sea level pressure: isobars, winds vectors) as derived over three successive WRF-ARW-AUTh forecasts covering the Mediterranean Sea (upper; domain d01), the Central Mediterranean (middle; domain d02) and the Central Macedonia (lower; domain d03) at 12:00 UTC on 25/01/19. The initial time of this forecast was at 12:00 on 24/01/2019. The red boxes mark the exact location of domains d02 and d03 in d01 and d02, respectively.

- Outflow of Aliakmonas river dams: estimated from electric power production data and the daily degree of reservoir filling rates (ADMIE 2024).

More detail on the HEC-HMS implementation and the evaluation of simulated freshwater outflows against in situ measured flow rates of Aliakmonas River can be found in Frysali et al. (2023).

2.3. Hydrodynamic circulation forecasts

The circulation simulations are based on the FLOW module of the Delft3D (Delft3D-FLOW; Deltares 2024a) modelling suite. The model is implemented by sigma-layer configuration in the vertical, covering the TG (Delft3D-Thermaikos) with a curvilinear grid (100 × 126) of varying spatial resolution, from 700 m in the southern to 300 m in the northern basin, to allow for higher resolution in the coastal shallower regions (Figure 1b; Androulidakis et al. 2021; Androulidakis et al. 2023a). The Delft3D-Thermaikos model solves the non-linear shallow water equations, derived from the Navier-Stokes equations for incompressible free-surface flow (Gerritsen et al. 2007). The boundary conditions, i.e. physical properties in the water column along the open southern boundary of the model with the Aegean Sea (Figure 1b), are derived from the Mediterranean Forecasting System (MFS 2024; Clementi et al. 2019; Coppini et al. 2023), distributed through the CMS Mediterranean Sea Physics Reanalysis dataset (Simoncelli et al. 2019). The MFS dataset, used in Wave4Us, is the MEDSEA_ANALYSISFORECAST_-PHY_006_013 that consists of hourly physical variables over the entire water column (~4 km horizontal resolution; 141 vertical sigma layers). The meteorological forcing consists of 3-hourly fields of zonal and meridional wind components, sea level pressure, air temperature, relative humidity, cloudiness, and precipitation, derived from the WRF-ARW-AUTh model (see Section 2.1). The freshwater input of Delft3D-Thermaikos is based on the discharge rates predicted by HEC-HMS (see Section 2.2). For the Axios and Aliakmonas river sources, the freshwater influxes (typically the highest in the domain) are introduced over 8 and 3 model cells, respectively, to better represent the deltaic discharges. The Delft3D-Thermaikos simulation provides 3-hourly forecasts of physical properties for the entire water column (e.g. temperature, salinity, density, currents). Androulidakis et al. (2021; 2023a) discussed in detail the model setup (e.g. initial, boundary, and forcing conditions; parameterizations and riverine freshwater input) and its performance, based on in situ measurements (for salinity, temperature, and Eulerian current velocities), satellite observations, and Lagrangian drifters (ocean currents and tracking pathways).

2.4. Storm surge and tide forecasts

The numerical simulation of the barotropic hydrodynamics is based on the High-Resolution Storm Surge (HiReSS) numerical model, developed in the LMEMW in AUTh (de Vries et al. 1995; Krestenitis et al. 2011). HiReSS simulates the 2-D barotropic mode of the hydrodynamic circulation in large water bodies, enclosed seas, gulfs, and coastal areas over a shoaling continental shelf, based on the shallow water equations (Makris et al. 2019). HiReSS takes into account several combined processes, such as the inverse barometer effect (response of sea level to atmospheric pressure gradient of large barometric systems), shear stresses of wind applied on the air–sea interface, geostrophic Coriolis forces on large water masses, astronomical tides, ocean bottom friction, and turbulence of horizontal vortices through the eddy viscosity parameterisation. The TG domain of HiReSS has a spatial resolution of approximately 1.67 km and considers the effects of astronomical tides on barotropic circulation through a static model parameterisation (Schwiderski 1980; Krestenitis et al. 2015; Androulidakis et al. 2023c). The latter follows a formulation that combines the equilibrium tidal potential with the self-attraction/loading effect under specific coefficient parameterizations (Matsumoto et al. 2000; Sakamoto et al. 2013; Makris et al. 2021). Meteorological forcing (atmospheric pressure and winds) is derived from the WRF-ARW-AUTh forecasts over the TG (domain d03; Figure 3; see Section 2.1). The HiReSS forecasts over the TG receive boundary conditions (sea level and barotropic currents) by a broader application of the HiReSS model over the Aegean Sea (http://coastal.web.auth.gr/ssm_Aeg_forecast.htm) that is also forced at its southern boundary from a respective Mediterranean Sea application (http://coastal.web.auth.gr/ssm_Med_forecast.htm; Androulidakis et al. 2023c). Both the Aegean and Mediterranean HiReSS simulations are forced by the respective WRF-ARW-AUTh applications' outputs (domains d01 and d02 in Figure 3; Section 2.1) over the same domains. The Sea Level Height (SLH) forecasts provide information about potential storm surges or sea level depressions, especially during low atmospheric pressure systems that may affect the TG's coastal zone. SLH forecasts are also used for the coastal inundation predictions of the Wave4Us platform (see Section 2.6). Further description of the mathematical equations and thorough validation of the HiReSS model against satellite and field observations can be found in Krestenitis

et al. (2011; Krestenitis et al. 2015; Krestenitis et al. 2017), Androulidakis et al. (2015, 2023c), and Makris et al. (2016; Makris et al. 2019; Makris et al. 2021; Makris et al. 2023a).

2.5. Wave forecasts

The predictions of wave train characteristics (significant wave height, H_s; peak spectral period, T_p; mean direction of irregular wave propagation, φ_w) are based on simulations with WaveWatch-III (WW-III). The model is a well-documented and widely implemented 3rd generation model for wind-generated spectral waves by the Marine Modeling and Analysis Branch of the NCEP. Its modules solve the wave-action balance equation based on the wave variance density spectrum and intrinsic wave frequency (Bretherthon and Garrett 1968). WW-III can simulate spectral wave shoaling and refraction due to changes in the mean water depth and current velocities. It further considers several physical processes, e.g. wind-induced wave growth, nonlinear wave-wave interactions, resonance in semi-enclosed basins, offshore wave energy dissipation (white-capping effect), depth-limited wave breaking, wave energy decay and scattering due to wave-bottom friction (WW3DG 2016). The incorporation of WW-III in the forecasting platform also follows a nested approach, with two levels of implementation over the Aegean Sea and the TG domain, with the same resolution as HiReSS (Section 2.4). Hourly wind forcing is provided by WRF-ARW-AUTh outputs (Section 2.1; domains d02 and d03 shown in Figure 3).

The WW-III simulations use a cold-start initiation (i.e. calm conditions) with a respective warm-up period to ensure a fully developed sea regime, and further incorporate the Ultimate Quickest numerical scheme (Tolman 2002) and a stability correction algorithm (Abdalla and Bidlot 2002). Depth-limited wave energy dissipation follows the classic Battjes and Janssen (1978) wave-breaking concept assuming that the total irregular wave energy dissipation is distributed over the entire spectrum so that it does not change the spectral shape (Eldeberky and Battjes 1996), while the bottom friction is tuned for JONSWAP spectra in shallow waters according to Tolman (1991) (WW3DG 2016). The white-capping effect, which is fairly evident in semi-enclosed seas (Shao et al. 2023), such as the TG, especially when typical local aeolian patterns (e.g. Vardaris, a regional offshore blowing ravine wind) prevail, is also parameterised because it can result in choppy sea waves and may affect local maritime transportations. Following the concept of Rogers et al. (2012), waves that break when they exceed a generic steepness to add to the

cumulative dissipative effect due to breaking are included. Triad and quadruple wave-to-wave resonant interactions are considered by means of a Discrete Interaction Approximation (DIA) in version 3.14 (Tolman 2008). Note that the swell regime in the northern Aegean Sea, specifically in the naturally protected semi-enclosed TG, is not particularly strong or significant compared to other exposed regions of the Mediterranean. Local wind conditions play a more critical role in wave generation than distant swells in the Gulf, which is influenced by seasonal wind patterns, such as the Etesian winds (also known as Meltemia) in the summer or local winds (e.g. Vardaris), that can cause choppy wave conditions locally. However, these conditions are more related to wind-driven waves rather than long-period swells generated in the open ocean. As noted in Soukissian et al. (2008), relatively short fetch durations and lengths and relatively low swells are characteristic features of the Aegean Sea, especially along the north-to-south, east-to-west and vice versa directions. Furthermore, Emmanouil et al. (2016) in their high-resolution study of wind, sea waves and wave energy assessment in the Aegean have shown that the Cyclades islands' domain in the Aegean Archipelago reduces the aeolian potential (wind speeds) in the area and further does not allow the swell to cross the region of the central Aegean, from south to north, creating a shadow effect on the leeward side of the islands. They also pinpoint that the wave power potential, related to swell seas, is minuscule in the TG based on their analysis of mean/max values, their standard deviations, kurtosis, etc. Comparisons with satellite observations are provided in Appendix A. The Wave4Us system also provides information on the wave conditions based on the Douglas Sea Scale for navigation and marine weather conditions.

2.6. Coastal flooding forecasts

The coastal inundation service is a new addition to the Wave4Us platform, providing estimations of the potential flooding under combined SLH (from the HiReSS model; Section 2.4) and wave-induced setup (from the WW-III model; Section 2.5) conditions over the coastal zone of TG. The potential seawater elevation refers to a representative value of the integrated sea level elevation at the shoreline for each discrete forecast timeframe (i.e. a 3-hourly integral). The WW-III model output refers to a characteristic 3-hourly value for each of the H_s, T_p, φ_w, representative of a mixed seas regime. These features feed the calculation of the wave setup (WS) in order to add it to the SLH derived from the HiReSS model. The WS is calculated separately by the semi-analytic

approach for the transformation of random wave characteristics from offshore to shallow coastal waters provided by Galiatsatou et al. (2019). The input of the necessary wave characteristics (H_s, T_p, φ_w) is provided by the WW-III forecasts on the last coastal cell of the spectral wave model. Therefore, one assessment of the single highest possible Total Water Level (TWL=SLH+WS) on the coast is produced every 3 hours to force the CoastFLOOD simulations, which in turn produce estimations of potential inundation of the littoral zone around the TG.

CoastFLOOD (Makris et al. 2023a) is a hydraulic model for seawater overland inundation running on very fine grid (2-5 m) on the inland coastal areas (Figure 1c). CoastFLOOD is a lowered complexity, shallow water equation, hydraulic flood flow model, operating on arbitrary land-elevation features for the 2-D simulation of coastal inundation over complex inland terrains (Bates et al. 2010). It uses the raster-based concept of depth-averaged, 2-D horizontally decomposed, mass balance, Manning-type flow equations over five discrete fine rectangular grids of Digital Elevation or Digital Surface Models (DEM or DSM) for the natural or artificial settings of the study area, respectively. The TG floodplains contain agricultural farmlands, estuaries, small lagoons/ponds, and beaches (Skoulikaris et al. 2021; Androulidakis et al. 2023c) or coastal urban sites, engineered waterfronts, port areas, etc. (Makris et al. 2023a; Androulidakis et al. 2023b).

CoastFLOOD can provide estimations of the possible extent of flood inundation over coastal low-land areas, the local seawater height above the inundated ground, and the maximum floodwater velocities around buildings, at property-level, on roads and other open spaces (Makris et al. 2024b). The model considers the wetting and drying of each computational grid-cell during the integration process on a von Neumann neighbourhood square grid with a meridional to zonal direction breakdown of the flow locally. Computations are programmed to stop when the farthest possible flooded cell away from the shoreline boundary is reached, i.e. the model is not allowed to simulate the retreat of seawater back to the marine environment to save computational time. The flow rates over each cell and at any direction are influenced by an effective Manning-type bottom friction approach calibrated by the fine-scale local characteristics of terrain roughness. Based on a variety of sources in the relevant technical literature, an all-inclusive list of Manning coefficient, n, values is created, by discretizing 43 classes (Makris et al. 2024b) obtained as a best-match to the Corine Land Cover CLC-2018 data codes.

The implemented land-elevation raster is produced by the highest resolution available geospatial datasets from the official DEM/DSM of the Hellenic Cadastre on a GGRS87 projection. The TG has historically experienced coastal erosion, particularly along sandy shores, with some areas seeing changes of several metres per year. However, most of the coastline remains stable due to natural protection. Significant shoreline modifications have resulted mainly from human interventions, such as the airport runway extension (2010–2015), but these changes have already been incorporated in the latest available high-resolution DEM (Hellenic Cadastre, 2024) used in our system. In general, short-term storm surges and sea level forecasts from the Wave4Us platform are not significantly affected by gradual erosion patterns, as the primary drivers of coastal flooding are extreme weather events. If erosion rates exceed several metres per year, DEM updates every five years are recommended, but the upgrades of national DTM products by the Hellenic Cadastre are scheduled only every ten years (the next one after 2026-2027).

Simulations consist of scenario-based runs of the most hazardous situation, i.e. high sea level on the coastline, within a 3-hour timeframe to simulate large-scale inundation due to sea level elevation (not an actual flood wave simulation of the second-to-second or minute-to-minute movement of seawater runup or overtopping on the coastal boundary and waterfront). It is further noted that the inundation model does not account for floodwater transpiration, ground infiltration or flow in subterranean sewage networks. However, it can consider most of the topographical peculiarities of the potentially flooded terrain in the coastal zone, such as engineered settings (urban infrastructure, buildings, roads, etc.) and natural floodplain formations (farmlands, forested areas, bare or stony lands, pastures, etc.) (Murdukhayeva et al. 2013; Kahl et al. 2024).

2.7. Marine pollution forecasts

The most recently included service on the modelling chain of the Wave4Us system is based on the D-Particle Tracking Lagrangian module of the Delft3D suite (Delft3D-Part). It can estimate the dynamic evolution and the spatial (sub-grid scale) concentration and distribution of individual particles by following their tracks in time and it is forced by the Wave4Us hydrodynamic forecast outputs (Delft3D-Thermaikos; see Section 2.3). Delft3D-Part has been used in a variety of applications and areas to track different pollutants and tracers in the marine environment, such as plastic debris (i.e. Raimundo et al. 2020), wastewater discharges (i.e. Bleninger and Jirka 2004), oil spills (i.e. Wang et al.

2017; Marinho et al. 2021), dispersion of biochemical material (i.e. Pinton and Canestrelli 2020; Buccino et al. 2022), larval transport (i.e. Takeshige et al. 2015), losses at sea (i.e. Gonzalez et al. 2022), etc. More detailed information about the Delft3D-Part parameterizations is described in the model's manual (Deltares 2024b).

The model domain and grid are the same as the ones used for the hydrodynamics, covering the entire TG (Figure 1b). This service is provided to users on-demand, to predict the fate of tracers (Lagrangian particles) in the event of marine pollution accidents (e.g. oil spills), pollutant intrusion from land sources (e.g. flash floods and polluted freshwater input), and necessity of search and rescue actions in the marine environment. Depending on the substance characteristics, the model can be used to simulate (conservative or decaying) passive tracers (Tracer mode) or oil particles (Oil mode). The displacement of each particle consists of a deterministic part, accounting for advection (and potentially settling) and a stochastic part, expressing dispersion. As the magnitude of the latter is determined by the local dispersion and the time step in the model, while its direction is random, the method used is often referred to as the 'random walk method'. Characteristics such as the initial conditions of the release, the type of release (e.g. instantaneous or continuous), release point (e.g. location and depth), type and mass of pollutants (e.g. type of oil, mass, release rate), among others, can be parameterised accordingly, depending on the pollution event. In a continuous release the specified number of particles is distributed over the complete simulation time.

3. Results

The main hazards and environmental stressors of TG are related to pollution events (e.g. from activities related to agriculture, aquaculture, industry, residential infrastructure, marine transportation and ports), coastal flooding (by storm surges and waves) over low-lying areas, and formation of MHWs due to intense atmospheric heatwaves. Examples of such events, selected based on to (i) their importance in terms of the potential impact on the coastal environment and (ii) the availability of observations for comparison, are presented below, focusing on the predictive skill of Wave4Us. Satellite and field observation data were used. The former provides wider spatial coverage, but can generally have lower temporal resolution, meaning the measurements for a given location cannot provide continuous information (e.g. every few days or weeks, depending on the satellite's orbit and revisit time). The latter have

higher temporal resolution, often capturing data continuously or at very frequent intervals, however, covering much smaller areas, usually at localised points (e.g. buoys). The indicative events presented here are primarily associated with the on-demand forecasting products of the platform (coastal flooding, pluvial and fluvial flooding, pollution and oil spill tracking). Specifically, the analysed cases are:

- Succesive severe low-pressure system that evolved over the Central Mediterranean from the 22nd to the 27th of January 2019 (Foivos Storm; Kotroni et al. 2021) and affected almost the entire Greek territory, causing extensive landslides and floods (Kotroni et al. 2021). WRF-ARW-AUTh forecasts during the storm are presented in Section 3.1.1. The potential seawater inundation during the storm over the coastal areas of the TG was simulated by CoastFLOOD, using meteorological (WRF-ARW-AUTh), SLH (HiReSS) and wave (WW-III) modelling results, and is described in Section 3.1.2.
- An oil spill of approximately 5,000 m^2 that was detected in the northern part of TG (Thessaloniki Bay; Figure 1b), due to an oil mass release at the docking location of the permanent refinery supply pipeline outside the Port of Thessaloniki in the morning hours of November 4th, 2017. The accident received significant public attention (Ertnews 2017) and was also detectable by satellite ocean colour imagery. As the semi-enclosed Thessaloniki Bay is the most vulnerable area of the TG (Androulidakis et al. 2024a) due to limited water renewal (Androulidakis et al. 2023a), the impacts of such incidents could be detrimental to the marine and coastal system. The Wave4Us forecasts, related to the prevailing metocean conditions and the oil spill evolution, are presented in Section 3.2.
- A severe low-pressure system (Medicane Numa) evolved over the central Mediterranean between the 12th and 19th of November 2017, causing 21 fatalities and approximately US\$100·10^6 of damages in Greece (Toomey et al. 2022). Besides the direct hazards related to the storm (e.g. flash floods, strong winds), the increased precipitation rates led to large freshwaters discharge into the marine environment. Such intense inflows of riverine water may contain high concentrations of nutrients and other pollutants and, depending on the TG's prevailing thermohaline and hydrodynamic conditions, can lead to the formation of eutrophication events (Androulidakis et al. 2021). The simulated discharge rates during the event and the spreading of the riverine waters

in the TG are evaluated against satellite imagery in Section 3.3.

- MHWs are associated with increased seawater temperatures and may significantly impact marine life, coastal habitats, and economic activities in the coastal zone (e.g. mussel cultures). An episode of very warm waters can be characterised as a MHW in case of extreme seawater temperatures (e.g. exceeding the 90th percentile), maintained for a significant period of consecutive days (e.g. 5 days; Hobday et al. 2016). Especially for the area of the TG, long-term (40 years) measurements have shown that MHWs associated with significantly higher SST interannual trends (0.52°C/decade; Androulidakis and Krestenitis 2022) compared with general trends over the eastern Mediterranean Sea (0.40°/decade; Mohamed et al. 2019). The skill of the Wave4Us forecasting system at detecting such events in the coastal enviroment of the TG is evaluated using the Delft3D-Thermaikos forecasts during one year (2017; Section 3.4).

3.1. Extreme event prediction: The case of Foivos Storm

3.1.1. Storm prediction

Snapshots of the three WRF-ARW-AUTh model domains, showing the main characteristics of Foivos Storm at 12:00 UTC on 25/01/2019 are presented in Figure 3 (SLP, precipitation and winds). WRF-ARW-AUTh efficiently predicted the spatial distribution of the storm that affected the biggest part of the Mediterranean Sea and with very low-pressure levels in the Ionian Sea (<990 hPa; Figure 2a). The storm-induced high precipitation rates over the entire region and the southerly winds over the Aegean Sea, turning to southeasterlies over the TG, are also shown in Figure 3. The WRF-ARW-AUTh prediction of the low-pressure system agrees with the operational analysis of the European Centre for Medium-range Weather Forecasts (ECMWF), which showed a minimum SLP of around 987 hPa for the cyclone at the time of the forecast. The storm caused a severe barometric reduction of approximately 25 hPa during the storm (<995 hPa) over the TG on 24/01/2019, which was efficiently simulated by WRF-ARW-AUTh (Figure 4a). However, the model overestimated the peak intensity of the storm. The Mean Absolute Error (MAE) of the mean SLP at the meteorological stations of the Hellenic National Meteorological Service at the airport of Thessaloniki (40.517°N, 22.967°E), Greece (Figure 1b), was equal to 1.8 hPa during the entire month of January 2019 and the period of the storm (Figure 4a). The normalised RMSE was equal to 0.2%, while the statistically

significant (p_{Value}= R_P was almost 1 (0.98). The model overestimated the 2 m air temperature (Figure 4b) and the 10 m wind speed (Figure 4c) at this station (MAE>0), but it successfully predicted their temporal variability (R_p>0.78). Regarding the overestimation of the 10 m wind speed, one must keep in mind that the model values are instantaneous, while the observations have been derived from official SYNOP reports and they correspond to 10-min averaged values. Similarly, overestimation of the near-surface wind speed forecasts in Greece, produced by high resolution limited-area numerical weather prediction models, has generally been reported in the literature (e.g. Koletsis et al. 2016; Boucouvala et al. 2021; Kartsios et al. 2021). The MAE of the air temperature at the airport of Thessaloniki in the whole of January and in the period of Foivos Storm was equal to 2.0 °K and 1.7 °K, respectively (Figure 4b). The MAE of the 10 m wind speed at the same station was equal to 2.2 m/s in January 2019, but it increased to 2.5 m/s during the passage of the Foivos Storm (Figure 4c). The normalised RMSEs for air temperature and wind speed were less than 20%. It is noted that the model errors are generally lower than in other simulations of intense weather events in Greece (Matsangouras et al. 2014, 2016; Pytharoulis et al. 2016; Karacostas et al. 2018).

Figure 4d illustrates the statistical scores of the accumulated precipitation (in the forecast horizon of 12 to 36 hours, to exclude the model spin-up) at the airport of Thessaloniki in 6-hour and 24-hour intervals, using a threshold of 0.1 mm. This threshold discriminates cases with precipitation or no-precipitation. The threshold was chosen as low because of the small number of events with strong precipitation at this station. For example, there were only four cases with recorded 6-hour precipitation amount larger than 5 mm in January 2019. The scores of the 24-hour precipitation have not been calculated during the Foivos storm, because of the very small sample size. Regarding the 6hr precipitation during the storm, the Frequency Bias (FBIAS; as the number of predicted over the number of observed events, with an optimum value of one) of 0.91 indicates that the model slightly underestimates the number of the precipitation events. The Probability of Detection (POD; number of hits/ number of observed events) reaches 0.73, the False Alarm Ratio (FAR; number of false alarms/ number of predicted events) is equal to 0.2, while the accuracy of the model (Heidke Skill Score, HSS), taking into account the random chance, is 0.58. Similar results for POD and HSS are obtained for the 6-hour precipitation in the whole of January 2019, while there is a small overestimation of the number of events (FBIAS=1.15) and doubling of FAR (0.42),
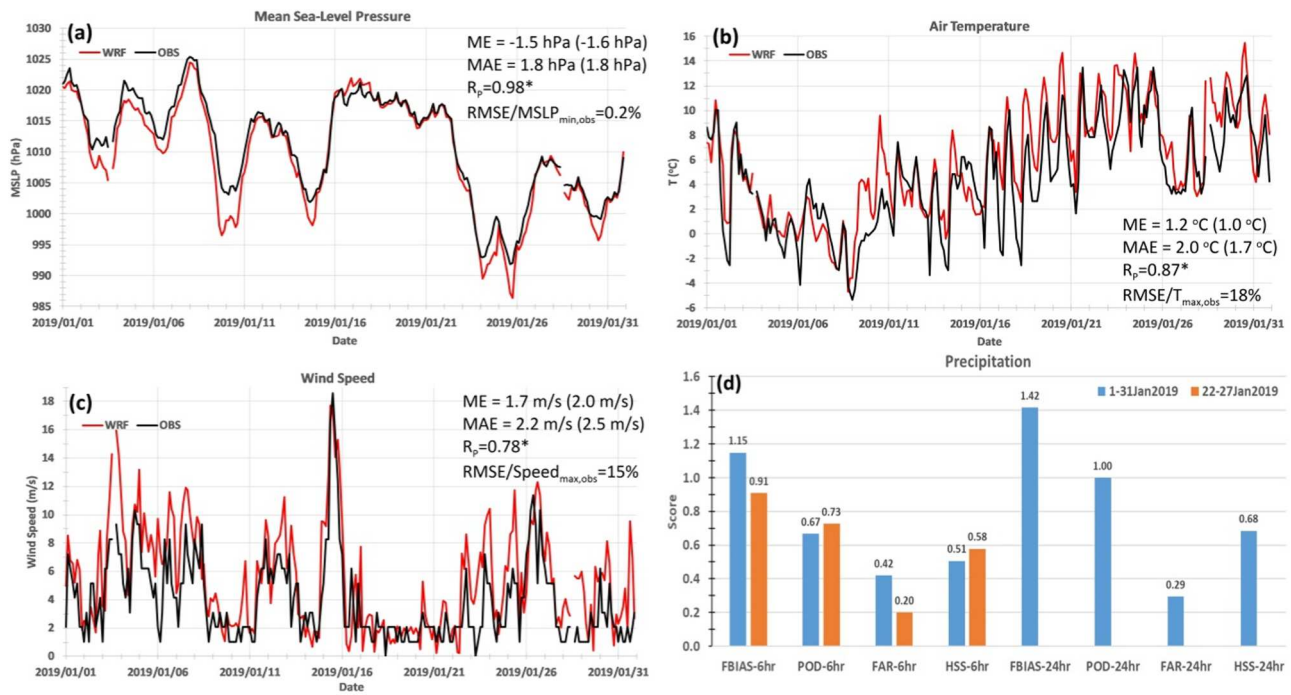
Figure 4. Timeseries of the 3hr predicted (WRF-ARW-AUTh; red line) and observed (black line) (a) mean sea-level pressure (MSLP; hPa), (b) 2 m air temperature (T; °C) and (c) 10 m wind speed (m/s) (all from 12 to 33 forecast hours) at the location of Thessaloniki Airport Station (LGTS, World Meteorological Organization number 16622) for January 2019 when a severe low pressure system occurred (from 22 to 27 January 2019). The Mean Error (ME; positive values denote overestimation by WRF-ARW-AUTh), the Mean Absolute Error (MAE), the Pearson Correlation Coefficient (R_P, *statistically significant value), and the normalised Root Mean Square Error (RMSE; with maximum observation for T and Wind Speed, and minimum observation for MSLP) for N = 246 pairs are also shown for the entire month of January 2019 and the period 22–27 January 2019 in brackets (48 pairs). (d) Statistical scores of Frequency Bias (FBIAS), Probability of Detection (POD), False Alarm Ratio (FAR) and Heidke Skill Score (HSS) of the 6hourly (6hr) and daily (24hr) precipitation amount for the entire January 2019 and 22–27 January 2019, at the threshold of 0.1 mm in the 12 to 36 hr forecast period.

compared to the storm period. Regarding the total amount of precipitation, the model predicted 69.43 mm (28.75 mm) in the whole of January 2019 (during Foivos storm, from 22 to 27 January) with an observed amount equal to 60 mm (38.8 mm). The prediction of the precipitation (occurrence, spatiotemporal distribution, intensity) is among the most challenging problems of numerical weather prediction. This is due to the complex processes which are involved at various spatial scales (from the large to the micro scale), the difficulty of the model parameterizations to accurately represent the moist processes, the errors in the input datasets used to define the physiographic characteristics (e.g. topography, land use) and the errors in the initial and boundary conditions. Ebert (2008) argued that although the high-resolution numerical forecasts look realistic and are very useful, they have difficulty predicting an exact match to the observations. The point error statistics are also influenced by temporal misplacements of the predicted precipitation, relative to the actual field. This is verified by the scores of the 24-hour accumulated precipitation in the whole January 2019 (Figure 4d) in which POD reaches its optimum value of one (which

means that all the observed events were predicted), FAR is reduced to 0.29 and HSS increases by 33% (relative to the 6hr scores) to 0.68.

3.1.2. Forecasting coastal inundation during the Foivos storm

Continuing with the same low-pressure atmospheric system that impacted the area in January 2019, we discuss the storm-induced flooding derived from Wave4Us predictions during the storm. The prevailing weather conditions (very low SLP<995 hPa; Figure 4a) gradually caused an increase of the SLH from around 0.3 m on the 24th of January, to over 0.4 m in the evening of the 25th (Figure 5b). Tide-gauge measurements from the station in Thessaloniki port confirm the simulated SLH variability during the storm (Figure 6a). The Pearson correlation coefficient (R_P) between the observed and predicted positive surges is R_P=0.67 (p_{value}<0.001), with RMSE=0.11 m and RMSE/$SLH_{max,obs}$=29%. However, the normalised mean error, derived for the two highest storm surge peaks on 24/01 and 25/01, is very low and equal to 1.2%. The storm surge induced by the system's passage over the area reached levels
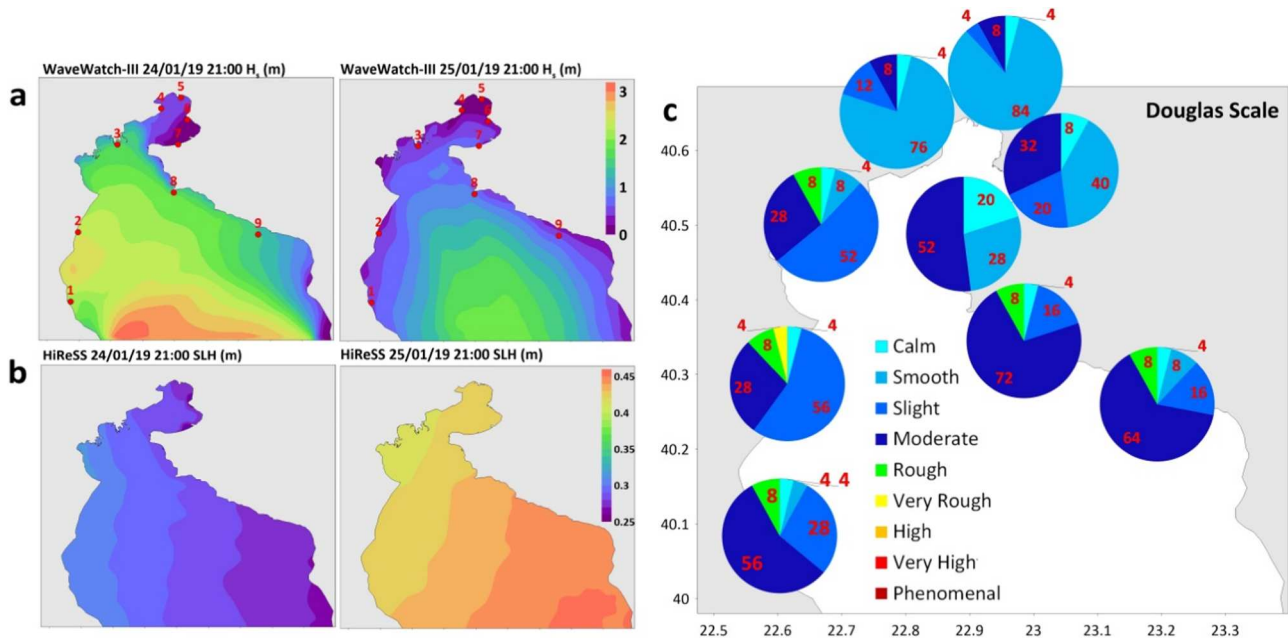
Figure 5. Distribution of (a) significant wave height (H$_s$; in m) by WW-III, and (b) Sea Level Height (SLH; in m) by HiReSS on 24/01/19 (left panels) and 25/01/19 (right panels). (c) Frequency (%) of Douglas sea scale degrees (1-9) for roughness of wave conditions at 9 areas along the TG's coastline for the period of the event. The locations of the 9 areas (clockwise numbering: 1 & 2: west coast of the outer TG, 3: Axios delta, 4: Gallikos delta, 5: Thessaloniki city, 6: Mikro Emvolo, 7: Peraia coast, 8 & 9: east coast of the outer TG) are marked in (a).

corresponding to the highest Storm Surge Index (SSI) recorded for the region (0.35–0.40 cm), as defined by Makris et al. (2016), using past and future climate projections. These surges, combined with wave-induced sea level increases, pose a significant threat to coastal lowland areas.

Increased wave heights were predicted for the evening of the 24th (one day prior to the SLP minima) at several areas of the TG domain, especially over the more exposed southern TG (H$_s$>2 m; Figure 5a). Based on the Douglas Sea Scale, the prevailing wave conditions over the southern gulf (<40.5°N) under the effect of southeasterly winds during the Foivos storm (24-27/01; Figure 3) were Moderate (>50%; Figure 5c), while 4% of Rough conditions also occurred. The TWL, derived from the combined storm surge and wave setup (see Section 2.6), varied significantly along the coast of the TG, with peak values on the 24th and 25th (Figure 6c). The highest TWLs were simulated for the evening of the 24th (>0.45 m) along the west coasts (over the Axios Delta and southwards), due to the combined effect of strong surges (∼0.3 m; Figure 6a) and especially high significant waves (2–3 m; Figure 6b), with lower TWLs over the northern coasts of the gulf (Figure 6c). The less exposed northern gulf showed Smooth wave conditions (<1 m; Figure 5c) and the TWL was mainly controlled by the SLH. A second TWL peak was captured on the 25th (Figure 6c), mainly

associated with the high SLH that affected the entire TG coastline (Figure 5b).

The different origins (wave or SLH) of the increased TWL played a role in the coastal inundation variability in the TG (Figure 7). The combined effect of storm- and wave-induced sea levels on January 24th inundated parts of the western coastal zone with significantly high floodwater levels (e.g. 0.6-0.8 m at Aliakmonas delta; Figure 7). Another inundated area, with lower flood heights (0.2 m), was detected in the vicinity of Macedonia Airport of Thessaloniki (eastern coast of Thessaloniki Bay). The next day (25/01; storm peak), the coastal flood effect was different, with the TWL mainly controlled by a generalised SLH increase, accompanied by lower wave heights along the north and west coasts (Figure 6b), conditions that led to weaker inundation over the deltas and more extended inundation over the eastern coast (floodwater height of 0.4–0.6 m; Figure 7). The total flooded area over the western and northwestern coasts (model domains A and B in Figure 1c) was reduced between the 24th and the 25th of January (Table 1), with an accompanying increase over the northeastern and eastern coasts (model domains C and D in Figure 1c). The largest total flooded area was computed on the 24th, covering approximately 18.6 km^2 (Table 1) of the northern TG coastal zone. These results testify to the ability of the Wave4Us platform in providing highly detailed estimations of both sea level conditions and
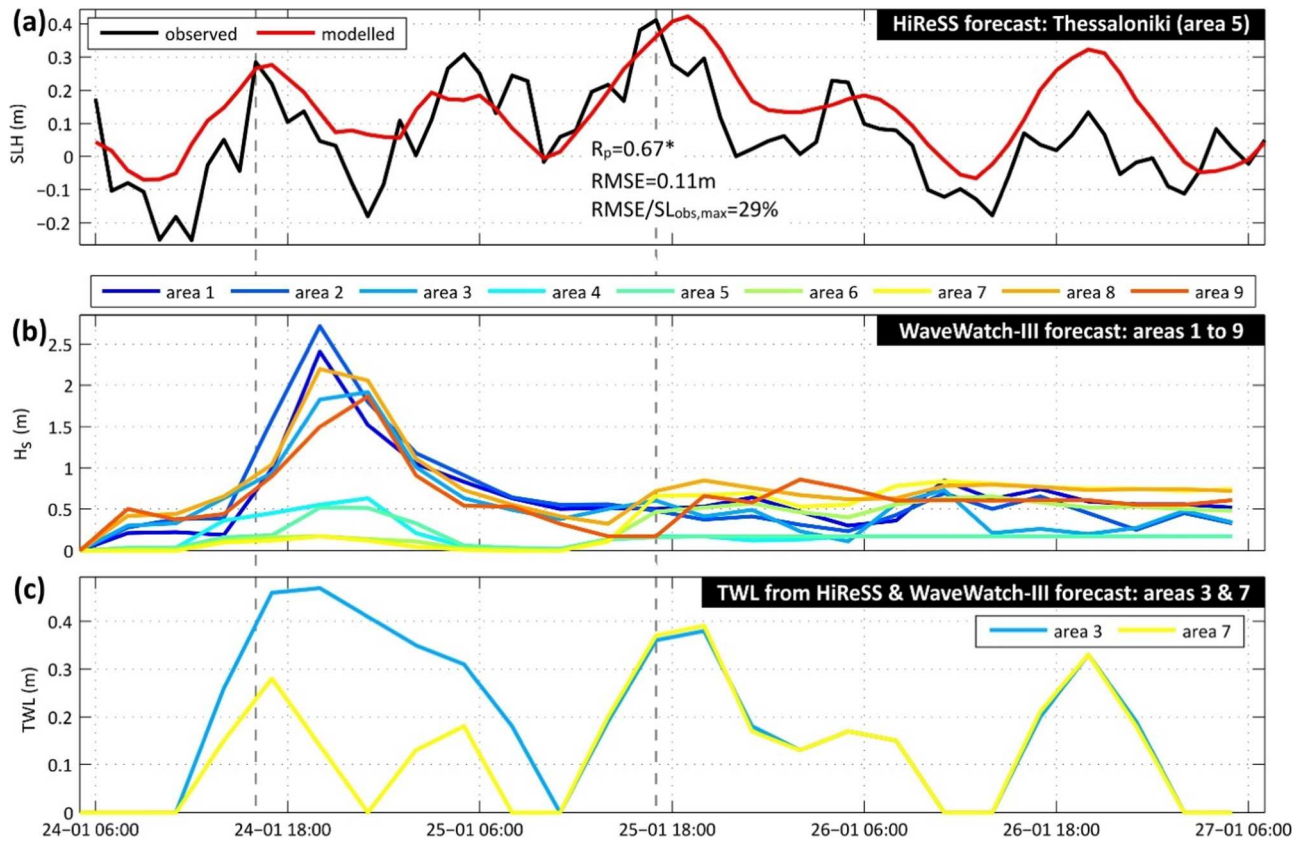
Figure 6. (a) Predicted (HiReSS) and measured (Tide-Gauge at Thessaloniki port; Figure 1c) Sea Level Height (SLH) at Area 5 (Thessaloniki; Figure 5) from 24/01/19 until 27/01/19. The Pearson correlation coefficient (R$_P$; *statistically significant value), the Root Mean Square Error (RMSE), and the normalised RMSE for the positive surges are shown. (b) Significant wave height (H$_s$) at 9 areas (Figure 5; clockwise numbering: 1 & 2: west coast of the outer TG, 3: Axios delta, 4: Gallikos delta, 5: Thessaloniki city, 6: Mikro Emvolo, 7: Peraia coast, 8 & 9: east coast of the outer TG) along the TG's coastline (WW-III). (c) Total Water Level (TWL) at Areas 3 and 7.

coastal flooding that may vary along the natural settings or built areas of the TG's coastline.

3.2. Oil spill accident in the northern TG

The simulated surface currents that prevailed during the oil spill accident in the northern TG are given in Figure 8a, when the prevailing southeasterly winds reached speeds over 9 m/sec (Figure 8b). Androulidakis et al. (2023a) showed that the general circulation of Thessaloniki Bay under southerly winds consists of a cyclonic pathway in the eastern part and an anticyclonic branch along the western coasts that both meet in the central area, forming a southward flow. The distribution of the surface currents on 05/11 (one day after the accident; Figure 8a) is consistent with this circulation pattern. The northward surface currents along the eastern and western coasts of Thessaloniki Bay during the event were between 0.1 and 0.2 m/sec (positive values in Section S1; Figure 8d) and the southward flow in the central bay and near the oil spill leak location was around 0.1 m/sec (negative values in Figure 8d). The

oil spill directly expanded southwards, following this central pathway, as verified by the ratio of Bands 2 and 11 (B2/B11; Kolokoussis and Karathanassi 2018) of Sentinel 2 L1C imagery, captured one day after the accident (05/11/2017; Figure 8c; Copernicus Data Space Ecosystem 2024; pixel size: 10 m).

The oil spill modelling during the same period assumed an Ekofisk type of oil and an initial oil mass equal to 10 t. The main characteristics of the Delft3D-Part set-up are presented in Table 2. The southward oil expansion during the first day after the release (Figure 8c) was adequately simulated by the oil spill model (Figure 8e). Oil patches were further transported by the prevailing anticyclonic circulation over the western part of the Thessaloniki Bay (Figure 8a) towards the northwestern shores (Figure 8e), where part of them (10% of the total mass) were stranded on the coasts, especially after 08/11 (Figure 8f). On 10/11, the floating oil mass in the sea was estimated to be less than half of the initial release (Figure 8f); the majority of the oil mass evaporated during the first 10 days. Note that precise information about the oil type, mass

Figure 7. Inundated areas and Flood Water Level (m; above land elevation), derived from the coastal flooding forecasts (CoastFLOOD) on 24/01/2019 21:00 and 25/01/2019 21:00 (left panels). Details over Area 7 (Macedonia Airport) during the same dates are also shown (right panels).

released, and possible mitigation measures applied after the accident would improve the accuracy of the simulations, but were not made available by the responsible company. Although the simulation results presented were based on assumptions for oil model characteristics, the integrated model suite provided efficient estimations about the prevailing circulation and the spreading of the oil spill.

**Table 1.** Daily maximum flood area (km²) for each of the four CoastFLOOD model domains (Figure 1c).

Model Domain	Maximum Flood Area (km²)				
	A	B	C	D	ALL
24/01/2019	5.59	11.65	0.26	1.73	18.61
25/01/2019	4.08	9.54	0.34	3.06	16.28
26/01/2019	3.18	6.16	0.29	2.87	12.49

3.3. Prediction of extreme freshwater outflow and spreading of riverine waters: The case of Medicane Numa

The increased precipitation rates during Medicane Numa (18-20/11/2017) significantly increased the freshwater discharges into the TG, especially for the Aliakmonas River (>200 m³/sec on 20/11/2017; Figure 9). The simulated freshwater outflows in the TG were evaluated against available flow rates, estimated through a stage-discharge curve and in situ measured stage data for the period of 2018 to 2020 (Appendix A; Figure A2; measurements for 2017 were not collected).

Figure 10a presents the river plume extension on 20/11/2017, based on the satellite-derived turbidity (Nephelometric Turbidity Units: NTU), derived from
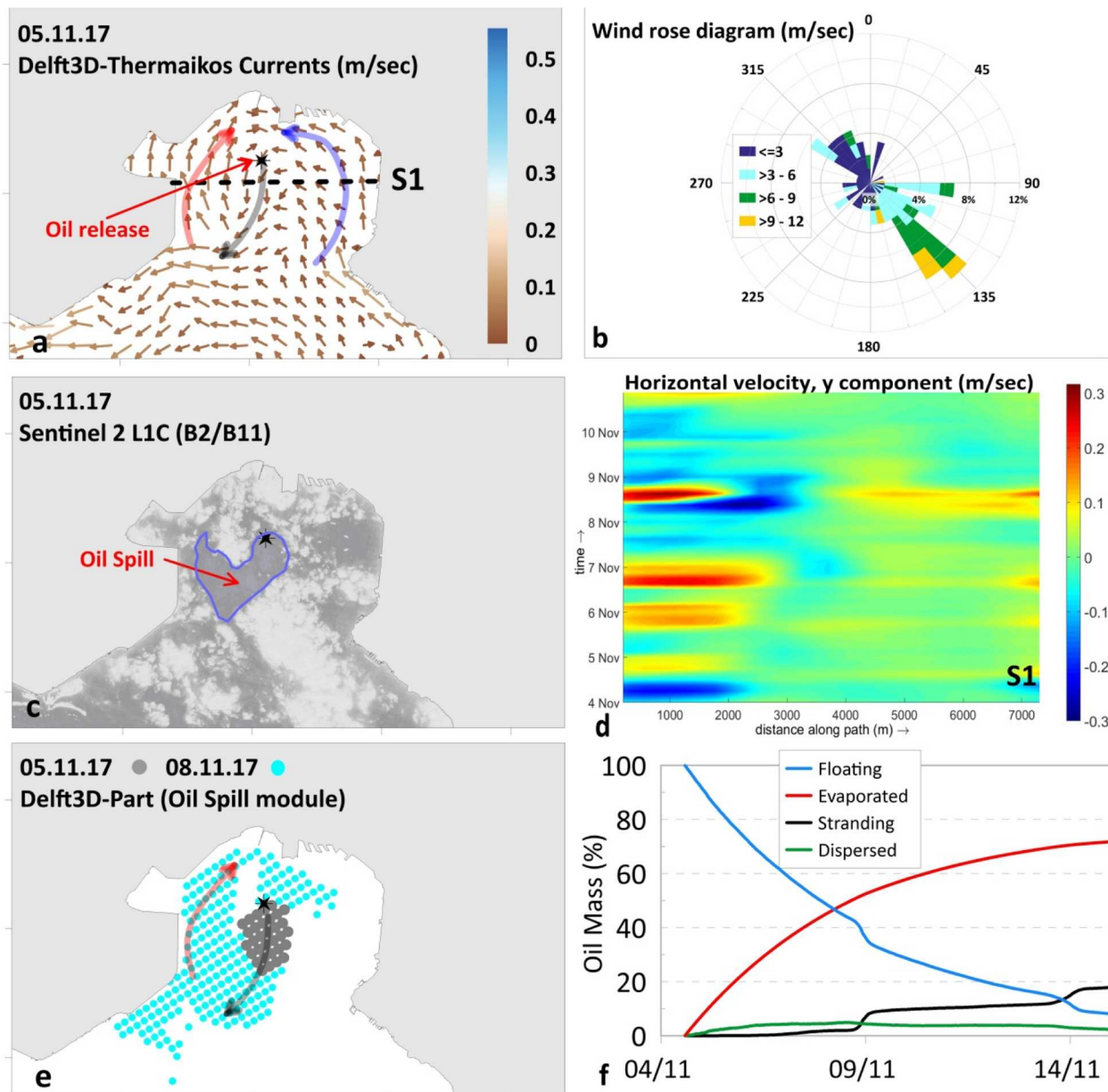
Figure 8. (a) Predicted surface currents (Delft3D-Thermaikos) on 05/11, (b) wind rose diagram (04-10/11/2017; WRF-ARW-AUTH), (c) observed oil spill (bands B2/B11) from Sentinel 2 L1C image on 05/11, (d) Hovmöller diagram (time-distance) of the meridional surface velocity (y component) across the S1 Section (04-10/11), (e) predicted (Delft3D-Part) oil spill on 05/11 (grey) and 08/11 (light blue), and (f) floating, evaporated, stranding, and dispersed fractions (%) of the total oil mass during 04/11-14/11. S1 section and the initial point of oil release are marked with a dashed black line and a black asterisk in panel (a), respectively.

Table 2. Characteristics of the oil model (Delft3D-Part).

Parameter	Value
Oil Type	Ekofisk
Oil mass (t)	10
Density (kg/m³)	890
Kinematic viscosity (cSt)	1500
Evaporation (1/day)	0.5
Maximum water content (0–1)	0.7
Stickiness probability (0–1)	0.5
Fraction at which emulsification starts	1
Emulsification parameter	2×10^{-6}
Volatile fraction (0–1)	0.94

an algorithm that was introduced and tested by Amran and Daming (2023); the model uses Bands 2 (blue), 3 (green) and 8 (NIR) of Sentinel 2 L1C, to estimate the coastal turbid waters that represent the river plume. The signal of the river plume is observed along the southwestern coasts (>4 NTU), while brackish waters were also detected over the central TG (~2 NTU; 40.4°N). The simulated salinity distribution, derived by the Delft3D-Thermaikos model, predicted these patterns, with salinity values of less than 37 along the
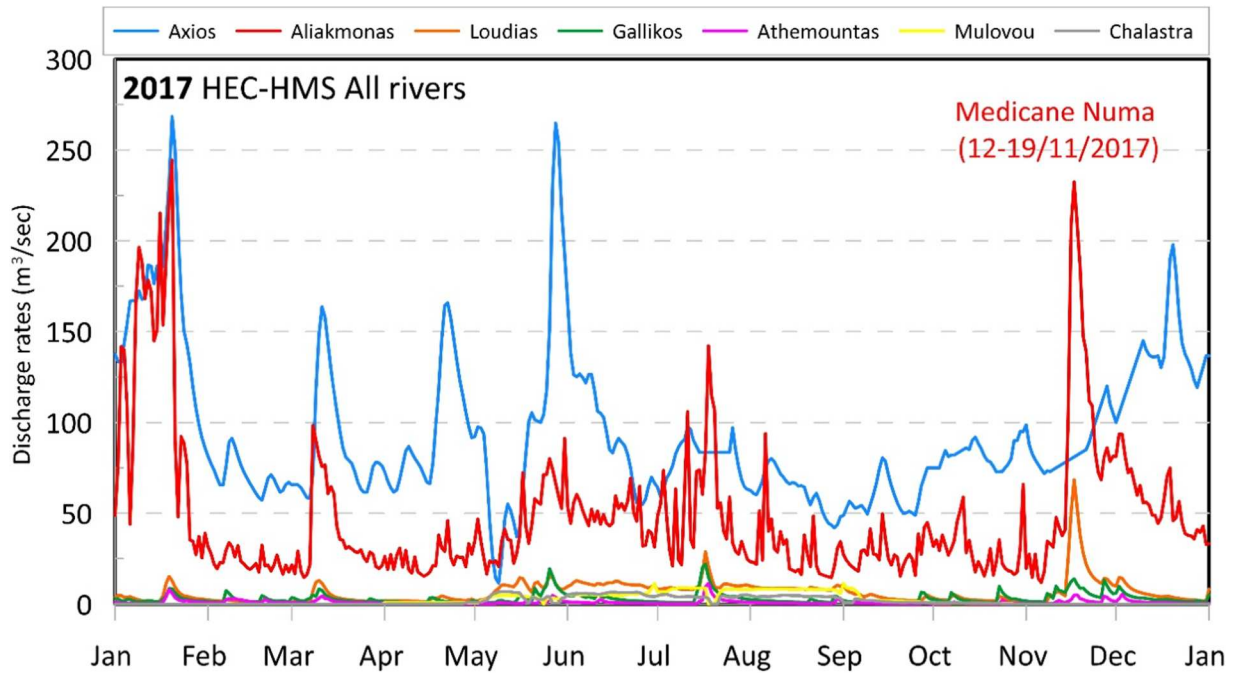
Figure 9. HEC-HMS simulated discharge rates (m³/sec) for all river sources presented in Figure 1b during 2017. The time period of Medicane Numa's impact is also marked.

western coast and a low salinity plume over the central TG (Figure 10b).

A continuous release of 25 tracers/hour (10,000 in total; passive, conservative and weightless) at the three main outflow channels of Aliakmonas delta was simulated using Delft3D-Part (Tracer mode) from 10/11 to 27/11. The tracer simulation aims to reproduce the physical connectivity between the release locations and the marine environment of the TG, while tracers are also allowed to move vertically through all 15 layers of the model grid (Delft3D-Thermaikos). The Lagrangian simulation shows that, by 20/11, the particles had spread over areas (Figure 10c) with high turbidity (Figure 10a) and low salinity levels (Figure 10b); the red lines in Figure 10c indicate the affected southwestern coastal zone, while particles were also detected offshore, in the central TG. The increased primary production during this period can be identified in the chlorophyll-a (chl-a) fields derived by high-resolution (1 km) satellite ocean colour images (Copernicus multi-sensor L4 product 2024; Volpe et al. 2018). The spreading of the nutrient-rich waters formed favourable conditions of increased primary production, which was relatively low before the storm period (10/11; Figure 10d) under lower river discharges (Figure 9). A chl-a increase was observed along the western coasts on 20/11 (Figure 10e) which became even higher (>4 mg/m³) a few days later (Figure 10f). The high levels detected in the offshore area of the southwestern TG (22.8°E; Figure

10f) also agree with the spreading of the simulated tracers (Figure 10c). The 4-day lag between the increased chl-a concentrations on 24/11 (Figure 10f) and the spreading of tracers on 20/11 (Figure 10c) over the southwestern TG is consistent with the phytoplankton growth timescales (doubling times on the order of days; Mann and Lazier 2006), and therefore, the time it takes for chl-a levels to increase in response to the introduction of nutrient-rich waters in the sea due to several factors: the concentration of nutrients, water temperature, light availability, and the presence of phytoplankton species capable of rapidly utilising the nutrients. Similar predictions with passive tracers can also guide search-and-rescue activities in the case of a loss (human or object) in the marine environment.

3.4. Predictions of Marine Heatwaves (MHWs)

The seasonal variation of the 90th percentile baseline, calculated with satellite-derived SSTs from 1982 to 2017 (Copernicus Reprocessed Mediterranean L4 dataset 2024; 0.05° resolution grid) and averaged over the TG, is presented in Figure 11, together with the respective daily variability of the observed and predicted (Delft3D-Thermaikos) SST during 2017 (time-series compiled by the first day of each daily forecast, as the most accurate prediction). According to the definition introduced by Hobday et al. (2016), an MHW is defined as a 'discrete and prolonged anomalously
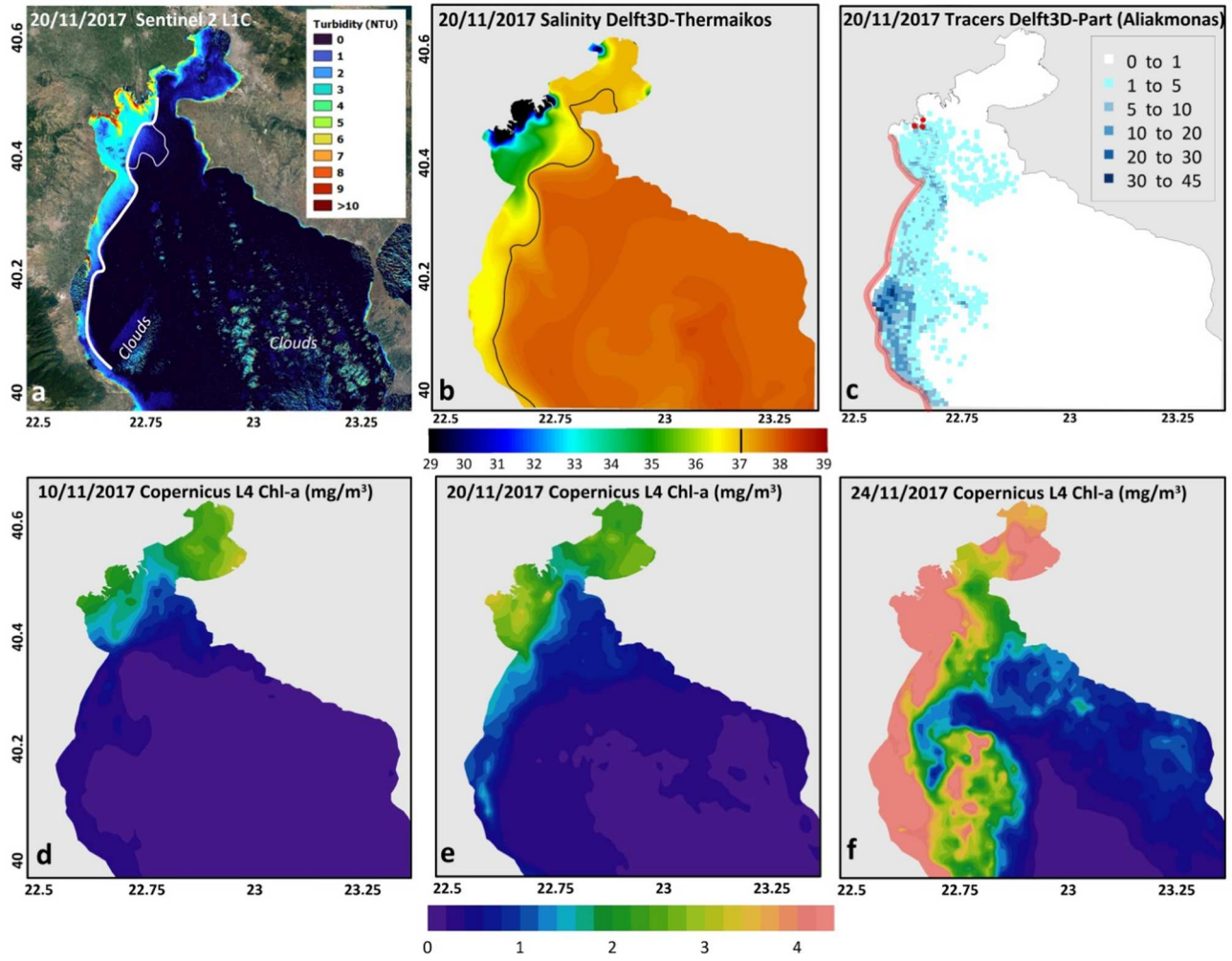
Figure 10. Distribution of (a) turbidity (NTU; Sentinel 2 1LC), (b) surface salinity (Delft3D-Thermaikos), and (c) surface passive tracers (Delft3D-Part; number of tracers) on 20/11/2017. Copernicus multi-sensor satellite-derived Chl-a concentrations (mg/m³) on (d) 10/11 (before), (e) 20/11 (during), and (f) 24/11 (after the storm). The location of particle release at the three main outflow mouths of Aliakmonas delta and the affected coastal zones are marked with red dots and lines, respectively, in (b).

warm ocean-based event'. The term 'discrete' implies that the MHW is an identifiable event, with clear start and end dates, and the term 'prolonged' means that it has a minimum period of days (three days in this case). 'Anomalously warm' means that the water temperature is warmer than the SST threshold (90th percentile climatological SST). The minimum MHW duration was set equal to three days, instead of the 5 days suggested by Hobday et al. (2016), so as to (a) increase the sensitivity of the method by including shorter episodes that may also have a significant impact on the enclosed coastal environment of TG, and (b) detect potential MHW events during the 3-day forecast timespan.

The observed and predicted SST variabilities show a very good agreement during the entire year ($R_P \approx 1.0$, RMSE=0.54°C, normalised RMSE≈2%), especially during the summer months, when the MHWs usually

occur; five MHWs were derived from the simulated values, showing similar mean intensities and durations (Table 3) as the observed events. The error between the observed and predicted SST values during the MHW events is from 0.25°C to 0.83°C; the normalised RMSE is less than 5% in all cases. The Cumulative Intensity (CI) of a MHW is determined by summing all daily intensities, which are the number of degrees above the SST threshold for those days Equation (1).

$$CI = \sum_{\iota=1}^{N} Daily\ Intensity \qquad (1)$$

where 'Daily Intensity' is the difference between the daily SST and the SST threshold and N is the MHW duration in days. The highest predicted and observed CIs were computed for Event#3 (Table 3), which occurred in late-June to early-July. The model seems
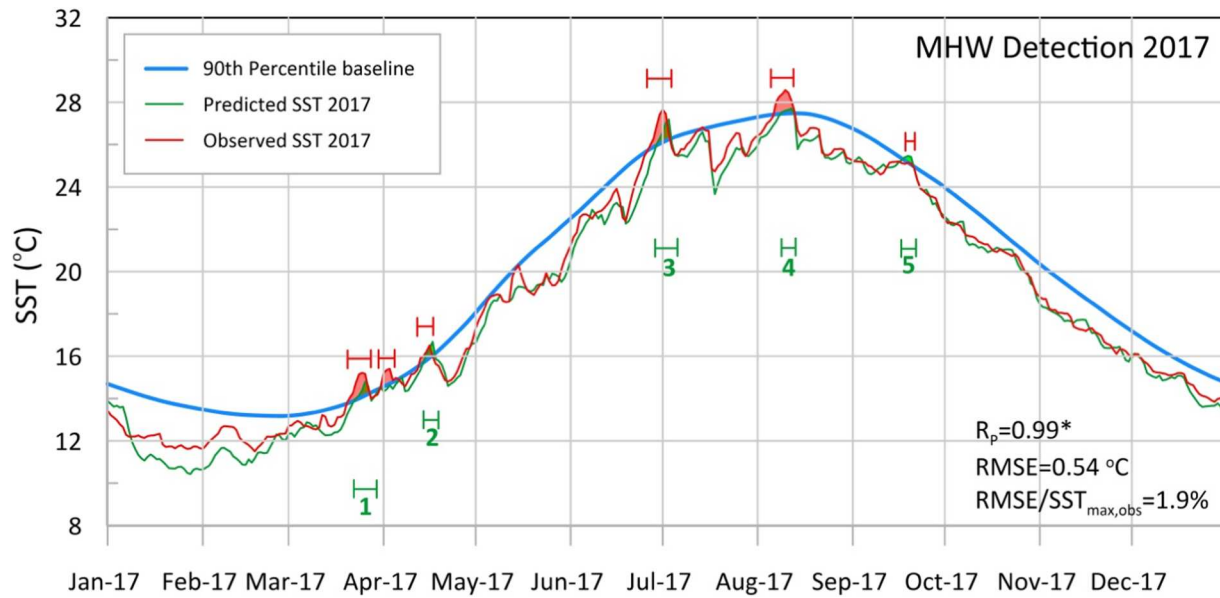
Figure 11. Observed (Satellite; red line) and predicted (Delft3D-Thermaikos; green line) Sea Surface Temperature (SST) with Marine Heatwave (MHW) events (1-5) for 2017 over TG. The SST 90th Percentile baseline, calculated from the satellite-derived 1982–2017 data, is also presented (blue line). The Pearson correlation coefficient (R_P; *statistically significant value), the Root Mean Square Error (RMSE) and the normalised RMSE with the maximum observed value, between the observed and simulated SST are shown.

to underestimate its CI (8.70 °C x days), mainly in terms of duration (4 days instead of 7). The mean intensity of Event#3 (2.40°C) was efficiently reproduced by the model (2.18°C; Table 3). The variability of SST, and thus the formation of MHWs, is determined by several met-ocean factors (e.g. radiation and heat fluxes, ocean circulation and vertical mixing processes) and its prediction is challenging, especially over topographically complex coastal areas such as TG. Improved air–sea fluxes (e.g. with even finer meteorological forecasts) or the increase of the vertical discretization of the hydrodynamic model may improve predictions. It is also noted that the available satellite observations of 0.05° that were used for the comparisons also reveal weaker accuracy over the coastal areas. Overall, five out of the six documented MHW episodes in 2017 (except for the early April event) were successfully detected by the model. The identification and the prediction of MHW in the TG are crucial, as the TG has been characterised as a hotspot of MHWs (Androulidakis and Krestenitis 2022; Androulidakis et al. 2024a; Androulidakis et al. 2024b) with strong biological implications on its ecosystem (Zgouridou et al. 2022).

4. Discussion and concluding remarks

The Wave4Us operational platform is a high-resolution forecasting system of meteorological and marine conditions over the Thermaikos Gulf (TG), serving a coastal zone of approximately 1.5 million residents (Thessaloniki is the second largest city in Greece). The services provided by the platform may have multiple applications. Wave4Us provides robust 3-day forecasts of the TG's sea state, circulation and thermohaline properties daily and can support a large range of activities related to the protection and management of the marine and coastal environment of the gulf. The predictions are open to the public, and specific on-demand forecasts can also be freely provided to responsible authorities within a few hours from the occurrence of an unfortunate event (e.g. pollutant release, oil spill, shipwreck or maritime accident loss at sea). Pollution events and other coastal hazards (e.g. storms, floods, MHWs) are quite common in the area, and their prediction contributes to the efficient mitigation of adverse effects on both the coastal environment and related ecosystem services and the population.

Other existing high-resolution coastal systems in the Mediterranean Sea (e.g. SOCIB, SAMOA, Accu-Waves, COASTAL CRETE, CYCOFOS, SELIPS, AEGIS) mainly focus on weather, ocean circulation, and/or wave conditions. The uniqueness of the system is also based on the targeted, high-resolution, meteorological forecasts over the TG that increase the performance of the metocean predictions, as well as allow to resolve local phenomena and processes that cannot be resolved by other well-known operational meteorological platforms (e.g. ICON, OpenSKIRON, ECMWF, Poseidon system) in Greek waters. Aside from enhancing the quality of meteorological forecasts, the high spatial

Table 3. Characteristics of the predicted (Delft3D-Thermaikos) and observed (Satellite) Marine Heatwaves (MHWs) during 2017.

A/A	MHW start	MHW end	Duration (days)	RMSE (°C)/ normalised RMSE (%)	Mean Intensity (°C)	Cumulative Intensity (°C x days)
	Predicted (Delft3D-Thermaikos)					
1	23/03/2017	27/03/2017	5	0.63°C /4%	1.23	6.13
2	15/04/2017	17/04/2017	3	0.33°C/2%	1.61	4.83
3	30/06/2017	03/07/2017	4	0.83°C/3%	2.18	8.70
4	09/08/2017	12/08/2017	4	0.76°C/2%	1.39	5.56
5	17/09/2017	21/09/2017	5	0.25°C/1%	1.46	7.31
	Observed (Satellite)					
1	21/03/2017	27/03/2017	7		1.61	11.26
2	13/04/2017	16/04/2017	4		1.54	6.17
3	27/06/2017	03/07/2017	7		2.40	16.79
4	07/08/2017	13/08/2017	7		1.96	13.73
5	19/09/2017	21/09/2017	3		1.32	3.95

resolution and holistic approach of Wave4Us sets it apart in terms of coastal predictions, compared to existing operational systems in the area (e.g. CMS, Poseidon System, ALERMO) that, being significantly coarser and typically employing climatological timeseries for freshwater fluxes, are unable to accurately reproduce the marine conditions in detail over morphologically complex coastal areas (e.g. enclosed gulfs, delta areas, straits). Wave4Us is the only coastal forecasting platform in Greece that includes a hydrological modelling component to provide near-real-time river discharges in the marine environment, thus being able to provide informed predictions of physical properties and thermohaline stratification in the gulf, parameters that are crucial for accurately describing the circulation patterns and dynamics in the domain (Krestenitis et al. 2012). The holistic approach followed here can be easily implemented in other coastal areas with similar characteristics.

Regarding the specialised forecasting products provided by the Wave4Us platform:

- Extreme freshwater outflows in the marine environment are a commonly underestimated hazard related to extreme weather events because riverine waters carry suspended solids, chemicals, nutrients, plastics and other debris. The pollution danger is especially intensified in the cases of flash floods, very common over ephemeral streams of continental Greece during severe storms. The pluvial and fluvial floodwater runoffs may carry different types of agricultural, urban, and industrial wastes over the inundated basins, leading them to the coastal ocean through the watershed network. Considering realistic freshwater discharges (HEC-HMS) has significantly improved model accuracies compared to using monthly climatological estimates only for the two main rivers (Krestenitis et al. 2014; Krestenitis et al. 2015) that were not able to reproduce the potential extreme outflows related to intense precipitation events. At the same time, the accurate reproduction of the weak outflow rates during the drier (e.g. summer) months is critical for the accurate simulation of the thermohaline circulation in the TG.

- Oil spill applications may support first-level responders to quickly implement measures for the restriction of the spill's expansion, reducing its consequences on marine and coastal habitats, as well as support hypothetical scenarios of oil releases and weather conditions that may provide valuable information of potential pollution risk zones and improve the preparedness of authorities. This service can be extremely useful for the northern TG (Thessaloniki Basin), with the presence of extensive oil-related infrastructure and heavy maritime traffic.

- The detection of vulnerable areas, where land-originated pollutants might spread after their discharge in the sea, in combination with the prevailing river-met-ocean conditions (e.g. discharge rates, winds, currents, stratification, etc.), can provide further estimations of possible eutrophication effects (e.g. red tides; Androulidakis et al. 2021) related to algal blooms in confined high-nutrient waters (Genitsaris et al. 2019).

- The operation of a coastal flooding model, coupled to the ocean sea level and wave simulations, provides estimations of potentially inundated littoral areas, especially during the passage of extensive low-pressure (deep depression) systems (Makris et al. 2023b) and could be used as an early warning system.

- The accurate prediction of MHWs is essential to support efforts to mitigate related ecological and socioeconomic implications and the adverse effects to the resilience of the TG's marine and coastal environment.

Integrating an operational biogeochemical model in Wave4Us would assist estimating the distribution of

biological and chemical variables and their impact on the ecological state of the gul, especially considering the significant repercussions of eutrophication events related to agricultural, industrial, and urban pollutants from several point and diffuse sources. Although the freshwater influxes to the TG from the main land sources are predicted by the current operating system, data on the freshwater quality of these discharges is not available, limiting the feasibility of such a prospect. An additional future step, which would require increased computational resources, is the development of additional forecast cycles (initialised with analyses of 00:00, 06:00 or 18:00 UTC, i.e. every 6 hours) that would update forecasts more frequently, improving the accuracy of forecast products. Finally, compound flooding from both sea and inland (e.g. precipitation, flash floods) waters will be included in the Wave4Us platform in the future, by coupling the existing HEC-HMS model with a fluvial/pluvial inundation model (e.g. HEC-RAS 2D with rain-on-grid approach) and the CoastFLOOD forecast outputs. The upgrade and improvement of the forecasting components of the platform is a continuous process, where further corrections and calibration of the models can be made using statistical techniques to reduce model bias (Lemos et al. 2020; Penalba et al. 2023). The Wave4Us operational forecast system is an innovative tool that aligns with the EU's strategic priorities for the establishment of digital twins in coastal regions until 2030. The integration of high-resolution model predictions is crucial for the efficient operation of the system and is a distinctive feature of Wave4Us. This capability can support coastal zone management practices by providing near real-time insights into coastal dynamics, thereby contributing to marine ecosystem resilience. By providing reliable local sea-state forecasts, it can empower stakeholders to make informed decisions, safeguarding the safety of coastal inhabitants, the ecological integrity, and the environmental health on a regional level of reference. At the same time, direct practical applications of forecasting products can be found in the marine renewable energy sector, with information that can assist proper planning of projects, not only in terms of energy potential (e.g. wave, wind, solar), as well as assessing their economic viability (e.g. for offshore wind farms the accessibility to the site for operation, maintenance and repairs is directly linked to metocean and visibility conditions; Konuk et al. 2023) and providing critical support to novel technologies, like production of energy from harvested marine plastic pollutants (Mallick et al. 2023; e.g. through the tracer application).

The environmental fragility of the TG, driven by a combination of intense anthropogenic pressures and the escalating impacts of climate change, has positioned the gulf as one of the Mediterranean's climate change hotspots (Androulidakis et al. 2024a; Androulidakis et al. 2024b). This underscores the critical need for reliable forecasting systems. Additionally, the model framework utilised in the Wave4Us system can be applied to evaluate the long-term future conditions of the gulf throughout the twenty-first century, using the latest updated climate scenarios. A risk-related framework is envisaged for the future based on a comprehensive statistical assessment, including extreme value analyses over long-term hindcasts, to quantify coastal hazards, exposure, vulnerability, resilience, and damage/impact costs for a proper risk assessment under an integrated coastal management perspective.

Acknowledgements

Disclosure statement

Funding

References

Abdalla S, Bidlot JR. 2002. Wind gustiness and air density effects and other key changes to wave model in CY25R1. Tech. Rep. Memorandum R60.9/SA/0273, Research Department, ECMWF, Reading, U. K.

ADMIE. 2024. Independent manager of electric energy transport, [accessed 2024 June 19]. https://www.admie.gr/agora/statistika-agoras/dedomena (in Greek).

AEGIS. 2024. Coastal environmental observatory for Northern Aegean. [accessed 2024 June 19]. https://aegis.aegean.gr/en/.

ALERMO. 2024. ALERMO Ocean forecasting system, [accessed 2024 June 19]. http://www.oc.phys.uoa.gr/oceanf.html.

Amran MA, Daming WS. 2023. Estimation of coastal waters turbidity using Sentinel-2 imagery. Geod Cartography. 49(4):180–185. doi:10.3846/gac.2023.18132.

Androulidakis Y, Kolovoyiannis V, Makris C, Krestenitis Y. 2024b. Evidence of 2024 summer as the warmest during the last four decades in the Aegean, Ionian, and Cretan Seas. J Mar Sci Eng. 12(11):2020. doi:10.3390/jmse12112020.

Androulidakis Y, Kolovoyiannis V, Makris C, Krestenitis Y, Baltikas V, Stefanidou N, Chatziantoniou A, Topouzelis K, Moustaka-Gouni M. 2021. Effects of ocean circulation on the eutrophication of a Mediterranean gulf with river inlets: The Northern Thermaikos Gulf. Cont Shelf Res. 221:104416. doi:10.1016/j.csr.2021.104416.

Androulidakis Y, Makris C, Kolovoyiannis V, Krestenitis Y, Baltikas V, Mallios Z, Pytharoulis I, Topouzelis K, Spondylidis S, Tegoulias I, Kontos Y. 2023a. Hydrography of Northern Thermaikos Gulf based on an integrated observational-modeling approach. Cont Shelf Res. 269:105141. doi:10.1016/j.csr.2023.105141.

Androulidakis Y, Makris C, Kombiadou K, Krestenitis YN, Stefanidou N, Antoniadou C, Krasakopoulou E, Kalatzi M, Baltikas V, Moustaka-Gouni M, Chintiroglou CC. 2024a. Oceanographic research in Thermaikos Gulf: a review over five decades. J Mar Sci Eng. 12(5):795. doi:10.3390/jmse12050795.

Androulidakis Y, Makris C, Mallios Z, Krestenitis Y. 2023b. Sea level variability and coastal inundation over the northeastern Mediterranean Sea. Coastal Eng J. 65(4):514–545. doi:10.1080/21664250.2023.2246286.

Androulidakis Y, Makris C, Mallios Z, Pytharoulis I, Baltikas V, Krestenitis Y. 2023c. Storm surges and coastal inundation during extreme events in the Mediterranean Sea: the IANOS medicane. Nat Hazards. 117(1):939–978. doi:10.1007/s11069-023-05890-6.

Androulidakis YS, Kombiadou KD, Makris CV, Baltikas VN, Krestenitis YN. 2015. Storm surges in the Mediterranean Sea: variability and trends under future climatic conditions. Dyn Atmos Oceans. 71:56–82. doi:10.1016/j.dynatmoce.2015.06.001.

Androulidakis YS, Krestenitis YN. 2022. Sea surface temperature variability and marine heat waves over the Aegean, Ionian, and Cretan Seas from 2008–2021. J Mar Sci Eng. 10(1):42. doi:10.3390/jmse10010042.

Bates PD, Horritt MS, Fewtrell TJ. 2010. A simple inertial formulation of the shallow water equations for efficient two-dimensional flood inundation modelling. J Hydrol. 387(1–2):33–45. doi:10.1016/j.jhydrol.2010.03.027.

Battjes JA, Janssen JPFM. 1978. Energy loss and set-up due to breaking of random waves. Proc 16th Int Conf Coastal Eng, ASCE. 32, 569–587. doi:10.1061/9780872621909.034.

Biolchi LG, Unguendoli S, Bressan L, Valentini A. 2021. Recent developments in the forecasting chain at Arpae-Simc for the Emilia-Romagna (Northeast Italy) coastal areas. In 9th EuroGOOS International Conference. 208–215.

Bleninger T, Jirka GH. 2004. Near-and far-field model coupling methodology for wastewater discharges (pp. 447–453). London: Taylor & Francis.

Boucouvala D, Andreadis T, Gofa F. 2021. Verification results for Greece. In "Verification of ICON in Limited Area Mode at COSMO National Meteorological Services", Rieger et al. (Eds), Reports on ICON, Issue 006, 9-12. Deutscher Wetterdienst, Offenbach, Germany. doi:10.5676/DWD_pub/nwv/icon_006.

Bretherthon FP, Garrett CJR. 1968. Wave trains in inhomogeneous moving media. Proc Roy Soc London, A. 302:529–554. doi:10.1098/rspa.1968.0034.

Buccino M, Daliri M, Buttarazzi MN, Del Giudice G, Calabrese M, Somma R. 2022. Arsenic contamination at the Bagnoli Bay seabed (South Italy) via particle tracking numerical modeling: pollution patterns from stationary climatic forcings. Chemosphere. 303:134955. doi:10.1016/j.chemosphere.2022.134955.

Chen F, Dudhia J. 2001. Coupling an advanced land surface–hydrology model with the Penn State–NCAR MM5 modeling system. Part I: model implementation and sensitivity. Mon Weather Rev. 129(4):569–585. doi:10.1175/1520-0493(2001)129<0569:CAALSH>2.0.CO;2.

Clementi E, Pistoia J, Escudier R, Delrosso D, Drudi M, Grandi A, Lecci R, Cretì S, Ciliberti SA, Coppini G, et al. 2019. Mediterranean Sea analysis and forecast (CMEMS MED-Currents, EAS5 system) [Dataset]. In: Copernicus Monitoring Environment Marine Service (CMEMS). doi:10.25423/CMCC/MEDSEA_ANALYSIS_FORECAST_PHY_006_013_EAS5.

CLMS. 2024. CLMS portfolio, [accessed 2024 June 19]. https://land.copernicus.eu/en/products?tab=explore.

COASTAL CRETE. 2024. A high-resolution COASTAL Forecasting system for CRETE Island, [accessed 2024 June 19]. https://marine.copernicus.eu/services/use-cases/coastal-crete-high-resolution-coastal-forecasting-system-crete-island.

Copernicus Data Space Ecosystem. 2024. [accessed 2024 June 19]. https://dataspace.copernicus.eu/.

Copernicus Marine Service. 2024. [accessed 2024 June 19]. https://marine.copernicus.eu/.

Copernicus multi-sensor L4 product. 2024. Mediterranean Sea, Bio-Geo-Chemical, L4, monthly means, daily gapfree and climatology Satellite Observations (1997-ongoing), [accessed 2024 June 19]. doi:10.48670/moi-00300.

Copernicus Reprocessed Mediterranean L4 dataset. 2024. Mediterranean Sea - High Resolution L4 Sea Surface Temperature Reprocessed, [accessed 2024 June 19]. doi:10.48670/moi-00173.

Coppini G, Clementi E, Cossarini G, Salon S, Korres G, Ravdas M, Lecci R, Pistoia J, Goglio AC, Drudi M, et al. 2023. The Mediterranean forecasting system – Part 1: evolution and performance. Ocean Sci. 19:1483–1516. doi:10.5194/os-19-1483-2023.

CORINE Land Cover. 2018. [accessed 2024 June 19]. https://land.copernicus.eu/en/products/corine-land-cover/clc2018.

CYCOFOS. 2024. Cyprus Coastal Ocean Forecasting and Observing System, [accessed 2024 June 19]. https://edmerp.seadatanet.org/report/8105.

Deltares. 2024a. Delft3D-FLOW: Hydro-Morphodynamics, User Manual V.4.5, February 2025) https://content.oss.deltares.nl/delft3d4/Delft3D-FLOW_User_Manual.pdf.

Deltares. 2024b. Delft3D-PART: Particle tracking, User Manual V.3.0, February 2025) https://content.oss.deltares.nl/delft3d4/Delft3D-PART_User_Manual.pdf.

de Vries H, Breton M, de Mulder T, Krestenitis Y, Proctor R, Ruddick K, Salomon JC, Voorrips A. 1995. A comparison of 2D storm surge models applied to three shallow European seas. Environ Softw. 10(1):23–42. doi:10.1016/0266-9838(95)00003-4.

Dimarchopoulou D, Keramidas I, Tsagarakis K, Markantonatou V, Halouani G, Tsikliras AC. 2024. Spatiotemporal fishing effort simulations and restriction scenarios in Thermaikos Gulf, Greece (northeastern Mediterranean Sea). Ocean Coast Manag. 247:106914. doi:10.1016/j.ocecoaman.2023.106914.

Ebert EE. 2008. Fuzzy verification of high-resolution gridded forecasts: a review and proposed framework. Meteorol Appl. 15:51–64. doi:10.1002/met.25.

EEA-10. 2024. Copernicus DEM, [accessed 2024 June 19]. https://spacedata.copernicus.eu/collections/copernicus-digital-elevation-model.

Eldeberky Y, Battjes JA. 1996. Spectral modelling of wave breaking: application to Boussinesq equations. J Geophys Res. 101:1253–1264. doi:10.1029/95JC03219.

Emmanouil G, Galanis G, Kalogeri C, Zodiatis G, Kallos G. 2016. 10-year high resolution study of wind, sea waves and wave energy assessment in the Greek offshore areas. Renew Energy. 90:399–419. doi:10.1016/j.renene.2016.01.031.

Ertnews. 2017. [accessed 2024 June 19]. https://www.ertnews.gr/ert3/thessaloniki/petreleokilida-entopistike-ston-thermaiko/ (in Greek).

European Commision. 2023. Europe's Digital Decade: digital targets for 2030, [accessed 2024 June 19]. https://commission.europa.eu/strategy-and-policy/priorities-2019-2024/europe-fit-digital-age/europes-digital-decade-digital-targets-2030_en.

European Soil Data Centre. 2024. 3D Soil Hydraulic Database of Europe at 1 km and 250 m resolution, [accessed 2024 June 19]. https://esdac.jrc.ec.europa.eu/content/3d-soil-hydraulic-database-europe-1-km-and-250-m-resolution.

Frysali D, Mallios Z, Theodossiou N. 2023. Hydrologic modeling of the Aliakmon River in Greece using HEC–HMS and open data. Euro-Mediterranean J Environ Integr. 8(3):1–17.

Galiatsatou P, Makris C, Prinos P, Kokkinos D. 2019. Nonstationary joint probability analysis of extreme marine variables to assess design water levels at the shoreline in a changing climate. Nat Hazards. 98:1051–1089. doi:10.1007/s11069-019-03645-w.

García-León M, Sotillo MG, Mestres M, Espino M, Fanjul EÁ. 2022. Improving operational ocean models for the Spanish Port authorities: assessment of the SAMOA coastal forecasting service upgrades. J Mar Sci Eng. 10(2):149. doi:10.3390/jmse10020149.

Genitsaris S, Stefanidou N, Sommer U, Moustaka-Gouni M. 2019. Phytoplankton blooms, red tides and mucilaginous aggregates in the urban Thessaloniki Bay, Eastern Mediterranean. Diversity. 11(8):136. doi:10.3390/d11080136.

Gerritsen H, de Goede ED, Platzek FW, van Kester JATM, Genseberger M, Uittenbogaard RE. 2007. Validation document Delft3D-FLOW, a software system for 3D flow simulations. The Netherlands: Delft Hydraulics. Report X, 356, p. M3470.

Gonzalez JRP, Escobar-Vargas J, Vargas-Luna A, Castiblanco S, Trujillo D, Guatame AC, Corzo G, Santos G, Perez LA. 2022. Hydroinformatic tools and their potential in the search for missing persons in rivers. Forensic Sci Int. 341:111478. doi:10.1016/j.forsciint.2022.111478.

HEC-HMS. 2024. Hydrological modeling system, US Army Corps of Engineers. [accessed 2024 June 19]. https://www.hec.usace.army.mil/software/hec-hms/.

Hellenic Cadastre. 2024. [accessed 2024 June 19]. https://www.ktimatologio.gr/.

Hobday AJ, Alexander LV, Perkins SE, Smale DA, Straub SC, Oliver EC, Benthuysen JA, Burrows MT, Donat MG, Feng M, Holbrook NJ. 2016. A hierarchical approach to defining marine heatwaves. Prog Oceanogr. 141:227–238. doi:10.1016/j.pocean.2015.12.014.

Iacono MJ, Delamere JS, Mlawer EJ, Shephard MW, Clough SA, Collins WD. 2008. Radiative forcing by long-lived greenhouse gases: calculations with the AER radiative transfer models. J Geophys Res: Atmos. 113: D13. doi:10.1029/2008JD009944.

Janić ZI. 2002. Nonsingular implementation of the Mellor–Yamada level 2.5 scheme in the NCEP Meso model. NCEP Office Note. 437:61.

Janjić ZI. 1994. The step-mountain eta coordinate model: further developments of the convection, viscous sublayer, and turbulence closure schemes. Mon Weather Rev. 122(5):927–945. doi:10.1175/1520-0493(1994)122<0927:TSMECM>2.0.CO;2.

Juza M, Mourre B, Renault L, Gómara S, Sebastián K, Lora S, Beltran JP, Frontera B, Garau B, Troupin C, Torner M. 2016. SOCIB operational ocean forecasting system and multi-platform validation in the Western Mediterranean Sea. J Operational Oceanogr. 9(sup1):s155–s166. doi:10.1080/1755876X.2015.1117764.

Kaberi H, Zeri C, Androulidakis Y, Varkitzi I, Siokou I, Zervoudaki S, Katsiaras N, Drakopoulou P, Tzempelikou E, Reizopoulou S, Bray L. 2023. Thermaikos Gulf: An Area Under Multiple Natural and Anthropogenic Pressures.

Kahl DT, Vulis LM, Schubert JE, Sanders BF. 2024. Characterizing longshore transport potential and divergence of drift to inform beach loss trends. Coastal Eng. 189:104473. doi:10.1016/j.coastaleng.2024.104473.

Karacostas T, Kartsios S, Pytharoulis I, Tegoulias I, Bampzelis D. 2018. Observations and modelling of the characteristics of convective activity related to a potential rain enhancement program in central Greece. Atmos Res. 208:218–228. doi:10.1016/j.atmosres.2017.08.014.

Karageorgis AP, Skourtos MS, Kapsimalis V, Kontogianni AD, Skoulikidis NT, Pagou K, Nikolaidis NP, Drakopoulou P, Zanou B, Karamanos H, Levkov Z. 2005. An integrated approach to watershed management within the DPSIR framework: Axios River catchment and Thermaikos Gulf. Reg Environ Change. 5:138–160. doi:10.1007/s10113-004-0078-7.

Kartsios S, Karacostas T, Pytharoulis I, Dimitrakopoulos AP. 2021. Numerical investigation of atmosphere-fire

interactions during high-impact wildland fire events in Greece. Atmos Res. 247:105253. doi:10.1016/j.atmosres.2020.105253.

Kendall M. 1975. Rank correlation measures, Charles Griffin. London. 202:15.

Koletsis I, Giannaros TM, Lagouvardos K, Kotroni V. 2016. Observational and numerical study of the Vardaris wind regime in northern Greece. Atmos Res. 171:107–120. doi:10.1016/j.atmosres.2015.12.011.

Kolokoussis P, Karathanassi V. 2018. Oil spill detection and mapping using sentinel 2 imagery. J Mar Sci Eng. 6(1):4. doi:10.3390/jmse6010004.

Kombiadou K, Krestenitis YN. 2012. Fine sediment transport model for river influenced microtidal shelf seas with application to the Thermaikos Gulf (NW Aegean Sea). Cont Shelf Res. 36:41–62. doi:10.1016/j.csr.2012.01.009.

Konuk EB, Centeno-Telleria M, Zarketa-Astigarraga A, Aizpurua JI, Giorgi G, Bracco G, Penalba M. 2023. On the definition of a comprehensive technology-informed accessibility metric for offshore renewable energy site selection. J Mar Sci Eng. 11(9):1702. doi:10.3390/jmse11091702.

Korres G, Lascaratos A, Hatziapostolou E, Katsafados P. 2002. Towards an ocean forecasting system for the Aegean Sea. The Global Atmos Ocean Syst. 8(2–3):191–218. doi:10.1080/1023673029000003534.

Kotroni V, Lagouvardos K, Bezes A, Dafis S, Galanaki E, Giannaros C, Giannaros T, Karagiannidis A, Koletsis I, Kopania T, Papagiannaki K. 2021. Storm naming in the Eastern Mediterranean: procedures, events review and impact on the citizens risk perception and readiness. Atmosphere. 12(11):1537. doi:10.3390/atmos12111537.

Krestenitis Y, Pytharoulis I, Karacostas T, Androulidakis Y, Makris C, Kombiadou K, Tegoulias I, Baltikas V, Kotsopoulos S, Kartsios S. 2017. Severe weather events and sea level variability over the Mediterranean Sea: the WaveForUs operational platform. In: Perspectives of Atmospheric Sciences (Eds: Karacostas, T., Bais, A., Nastos, P.T.), Springer Atmospheric Sciences, Springer International Publishing, COMECAP 2016 Proceedings, Pt.1: Meteorology, pp. 63–68.

Krestenitis YA, Kombiadou KA, Androulidakis Y, Makris CH, Baltikas VA, Skoulikaris CH, Kontos YA, Kalantzi GI. 2015. Operational oceanographic platform in Thermaikos Gulf (Greece): forecasting and emergency alert system for public use. In Proceedings of 36th IAHR World Congress. 28 June – 3 July 2015, The Hague, the Netherlands.

Krestenitis YN, Androulidakis Y, Kombiadou K, Makris C, Baltikas V, Kalantzi G. 2014. Operational oceanographic forecasts in the Thermaikos gulf: the WaveForUs project. In 12th International Conference on Protection and Restoration of the Environment (PRE). 313–318.

Krestenitis YN, Androulidakis YS, Kontos YN, Georgakopoulos G. 2011. Coastal inundation in the north-eastern Mediterranean coastal zone due to storm surge events. J Coast Conserv. 15:353–368. doi:10.1007/s11852-010-0090-7.

Krestenitis YN, Kombiadou KD, Androulidakis YS. 2012. Interannual variability of the physical characteristics of North Thermaikos Gulf (NW Aegean Sea). J Mar Sys. 96–97:132–151. doi:10.1016/j.jmarsys.2012.02.017.

Lemos G, Menendez M, Semedo A, Camus P, Hemer M, Dobrynin M, Miranda PM. 2020. On the need of bias correction methods for wave climate projections. Glob Planet Change. 186:103109. doi:10.1016/j.gloplacha.2019.103109.

Makris C, Androulidakis Y, Baltikas V, Kontos Y, Karambas T, Krestenitis Y. 2019. HiReSS: Storm Surge Simulation Model for the Operational Forecasting of Sea Level Elevation and Currents in Marine Areas with Harbor Works. Proceedings of 1st International Scientific Conference on Design and Management of Port Coastal and Offshore Works (DMPCO), Athens, Greece, 8-11 May 2019, Vol. 1, pp. 11–15.

Makris C, Androulidakis Y, Karambas T, Papadimitriou A, Metallinos A, Kontos Y, et al. 2021. Integrated modelling of sea-state forecasts for safe navigation and operational management in ports: application in the Mediterranean Sea. Appl Math Model. 89:1206–1234. doi:10.1016/j.apm.2020.08.015.

Makris C, Galiatsatou P, Tolika K, Anagnostopoulou C, Kombiadou K, Prinos P, Velikou K, Kapelonis Z, Tragou E, Androulidakis Y, et al. 2016. Climate change effects on the marine characteristics of the Aegean and Ionian Seas. Ocean Dynamics, Springer. 66(12):1603–1635. doi:10.1007/s10236-016-1008-1.

Makris C, Mallios Z, Androulidakis Y, Krestenitis Y. 2023a. CoastFLOOD: a high-resolution model for the simulation of coastal inundation due to storm surges. Hydrology. 10(5):103. doi:10.3390/hydrology10050103.

Makris C, Papadimitriou A, Baltikas V, Spiliopoulos G, Kontos Y, Metallinos A, Androulidakis Y, Chondros M, Klonaris G, Malliouri D, Nagkoulis N. 2024a. Validation and application of the accu-waves operational platform for wave forecasts at ports. J Mar Sci Eng. 12(2):220. doi:10.3390/jmse12020220.

Makris CV, Androulidakis YS, Mallios ZC, Kourafalou VH. 2024b. On Modeling the Coastal Floods and Assessing the Impacts on Inundated Urban Areas of Miami (FL, USA). Proceedings of the 34th International Ocean and Polar Engineering Conference (ISOPE), 16-21 June 2024, Rhodes, Greece.

Makris CV, Tolika K, Baltikas VN, Velikou K, Krestenitis YN. 2023b. The impact of climate change on the storm surges of the Mediterranean Sea: coastal sea level responses to deep depression atmospheric systems. Ocean Model. 181:102149. doi:10.1016/j.ocemod.2022.102149.

Mallick K, Sahu A, Dubey NK, Das AP. 2023. Harvesting marine plastic pollutants-derived renewable energy: a comprehensive review on applied energy and sustainable approach. J Environ Manag. 348:119371. doi:10.1016/j.jenvman.2023.119371.

Mann HB. 1945. Nonparametric tests against trend. Econometrica: Journal of Economic Sociecy. 13:245–259. doi:10.2307/1907187.

Mann KH, Lazier JRN. 2006. Dynamics of Marine Ecosystems. Biological–Physical Interactions in the Oceans. 3rd Edition, Black-well Publishing, 2006, 496 pages, ISBN 1405111186.

Marinho C, Nicolodi JL, Neto JA. 2021. Environmental vulnerability to oil spills in Itapuã State Park, Rio Grande do Sul, Brazil: An approach using two-dimensional numerical simulation. Environ Pollut. 288:117872. doi:10.1016/j.envpol.2021.117872.

Matsangouras I, Nastos PT, Pytharoulis I. 2016. Study of the tornado event in Greece on march 25, 2009: synoptic

analysis and numerical modeling using modified topography. Atmos Res. 169:566–583. doi:10.1016/j.atmosres.2015.08.010.

Matsangouras I, Pytharoulis I, Nastos PT. 2014. Numerical modeling and analysis of the effect of complex Greek topography on tornadogenesis. Nat Hazards Earth Syst Sci. 14:1905–1919. doi:10.5194/nhess-14-1905-2014.

Matsumoto K, Takanezawa T, Ooe M. 2000. Ocean tide models developed by assimilating TOPEX/POSEIDON altimeter data into hydrodynamical model: A global model and a regional model around Japan. J Oceanogr. 56:567–581. doi:10.1023/A:1011157212596.

Mellor GL, Yamada T. 1982. Development of a turbulence closure model for geophysical fluid problems. Rev Geophys. 20(4):851–875. doi:10.1029/RG020i004p00851.

MFS. 2024. Mediterranean Forecasting System, [accessed 2024 June 19]. http://medforecast.bo.ingv.it/.

Mohamed B, Abdallah AM, Alam El-Din K, Nagy H, Shaltout M. 2019. Inter-annual variability and trends of sea level and sea surface temperature in the Mediterranean Sea over the last 25 years. Pure Appl Geophys. 176:3787–3810. doi:10.1007/s00024-019-02156-w.

Murdukhayeva A, August P, Bradley M, LaBash C, Shaw N. 2013. Assessment of inundation risk from sea level rise and storm surge in northeastern coastal national parks. J Coast Res. 29(6a):1–16. doi:10.2112/JCOASTRES-D-12-00196.1.

Penalba M, Guo C, Zarketa-Astigarraga A, Cervelli G, Giorgi G, Robertson B. 2023. Bias correction techniques for uncertainty reduction of long-term metocean data for ocean renewable energy systems. Renew Energy. 219:119404. doi:10.1016/j.renene.2023.119404.

Pinton D, Canestrelli A. 2020. Understanding How the Release of E. coli and Nutrients from Septic Tanks into the Guana-Tolomato-Matanzas Estuary and the Adjacent Ocean Affect Human. Plant and Animal Health, pp. 1–35.

Poseidon System. 2024. Monitoring, Forecasting and Information System for the Greek Seas. [accessed 2024 June 19]. https://poseidon.hcmr.gr/.

Prochaska C, Zouboulis A. 2020. A mini-review of urban wastewater treatment in Greece: history, development and future challenges. Sustainability. 12(15):6133. doi:10.3390/su12156133.

Pytharoulis I, Karacostas T, Christodoulou M, Matsangouras I. 2021. The July 10, 2019 catastrophic supercell over northern Greece. Part II: Numerical modelling. In: Proceedings of the 15th International Conference on Meteorology, Climatology and Atmospheric Physics, 26-29 September, Ioannina, Greece. pp. 885–890.

Pytharoulis I, Karacostas T, Tegoulias I, Kotsopoulos S, Bampzelis D. 2015a. Predictability of intense weather events over northern Greece. In: Proceedings of 95th AMS Annual Meeting, 4-8 January, Phoenix, Arizona, USA.

Pytharoulis I, Kotsopoulos S, Tegoulias I, Kartsios S, Bampzelis D, Karacostas T. 2016. Numerical modeling of an intense precipitation event and its associated lightning activity over northern Greece. Atmos Res. 169:523–538. doi:10.1016/j.atmosres.2015.06.019.

Pytharoulis I, Tegoulias I, Kotsopoulos S, Bampzelis D, Karacostas T, Katragkou E. 2015b. Verification of the operational high-resolution WRF forecasts produced by WAVEFORUS project. In: Proceedings of 16th Annual WRF Users' Workshop, vols. 15–19. June, Boulder, Colorado, USA.

Raimundo GI, Sousa MC, Dias JM. 2020. Numerical modelling of plastic debris transport and accumulation throughout Portuguese coast. J Coast Res. 95(SI):1252–1257. doi:10.2112/SI95-242.1.

Rogers E, Black T, Ferrier B, Lin Y, Parrish D, DiMego G. 2001. Changes to the NCEP Meso Eta Analysis and Forecast System: Increase in Resolution, New Cloud Microphysics, Modified Precipitation Assimilation, Modified 3DVAR Analysis, vol. 488. NOAA/NWS Technical Procedures Bulletin, Washington, DC, USA. [accessed 2022 June 24]. http://www.emc.ncep.noaa.gov/mmb/mmbpll/mesoimpl/eta12tpb/.

Rogers WE, Babanin AV, Wang DW. 2012. Observation-consistent input and whitecapping dissipation in a model for wind-generated surface waves: description and simple calculations. J Atmos Oceanic Techn. 29:1329–1346. doi:10.1175/JTECH-D-11-00092.1.

Sakamoto K, Tsujino H, Nakano H, Hirabara M, Yamanaka G. 2013. A practical scheme to introduce explicit tidal forcing into an OGCM. Ocean Sci. 9(6):1089–1108. doi:10.5194/os-9-1089-2013.

SAMOA. 2024. Sistema de Apoyo Meteorológico y Oceanográfico de la Autoridad Portuaria. [accessed 2024 June 19]. https://www.puertos.es/es-es/proyectos/Paginas/SAMOA.aspx#.

Schwiderski EW. 1980. On charting global ocean tides. Rev Geophys. 18(1):243–268. doi:10.1029/RG018i001p00243.

SELIPS. 2024. South Eastern Levantine Israeli Prediction System. [accessed 2024 June 19]. https://isramar.ocean.org.il/isramar2009/selips/.

Shao Z, Liang B, Sun W, Mao R, Lee D. 2023. Whitecapping term analysis of extreme wind wave modelling considering spectral characteristics and water depth. Cont Shelf Res. 254:104909. doi:10.1016/j.csr.2022.104909.

Simoncelli S, Fratianni C, Pinardi N, Grandi A, Drudi M, Oddo P, Dobricic S. 2019. Mediterranean Sea Physical Reanalysis (CMEMS MED-Physics). Copernicus Monitoring Environment Marine Service. REANALYSIS_PHYS_006_004 (CMEMS) [Data set]. doi:10.25423/MEDSEA_.

Skliris N, Sofianos S, Mantziafou A, Lascaratos A. 2007. Ocean forecasting in the eastern Mediterranean, the ALERMO system. Rapp Comm Int Mer Mediterr. 72:198.

Skoulikaris C, Makris C, Katirtzidou M, Baltikas V, Krestenitis Y. 2021. Assessing the vulnerability of a deltaic environment due to climate change impact on surface and coastal waters: The case of Nestos River (Greece). Environ Model Assess. 26:459–486. doi:10.1007/s10666-020-09746-2.

SOCIB. 2024. Balearic Islands Coastal Observing and Forecasting System. [accessed 2024 June 19]. https://www.socib.es/data/.

Sotillo MG, Cerralbo P, Lorente P, Grifoll M, Espino M, Sanchez-Arcilla A, Álvarez-Fanjul E. 2020. Coastal ocean forecasting in Spanish ports: the SAMOA operational service. J Operational Oceanogr. 13(1):37–54. doi:10.1080/1755876X.2019.1606765.

Sotillo MG, Mourre B, Mestres M, Lorente P, Aznar R, García-León M, Liste M, Santana A, Espino M, Álvarez E. 2021. Evaluation of the operational CMEMS and coastal downstream ocean forecasting services during the storm Gloria (January 2020). Front Mar Sci. 8:644525. doi:10.3389/fmars.2021.644525.

Soukissian T, Prospathopoulos A, Hatzinaki M, Kabouridou M. 2008. Assessment of the wind and wave climate of the Hellenic Seas using 10-year Hindcast results. The Open Ocean Eng J. 1:1–12. doi:10.2174/1874835X00801010001.

Spanoudaki K, Zodiatis G, Kampanis N, Quarta ML, Folegani M, Galanis G, Nikolaidis M, Nikolaidis A. 2021. May. Coastal crete: a high-resolution operational forecasting system for the coastal area of crete, eastern mediterranean. In 9th EuroGOOS International conference. 245–252.

SWRI. 2024. Soil and Water Resources Institute, [accessed 2024 June 19]. https://www.swri.gr/index.php/en/.

Takeshige A, Miyake Y, Nakata H, Kitagawa T, Kimura S. 2015. Simulation of the impact of climate change on the egg and larval transport of Japanese anchovy (Engraulis japonicus) off Kyushu Island, the western coast of Japan. Fish Oceanogr. 24(5):445–462. doi:10.1111/fog.12121.

The WAVEWATCH III® Development Group (WW3DG). 2016. User manual and system documentation of WAVEWATCH III® version 5.16. Tech. Note 329, NOAA/NWS/NCEP/MMAB, College Park, MD, USA, 326 pp.

Tintoré J, Pinardi N, Álvarez-Fanjul E, Aguiar E, Álvarez-Berastegui D, Bajo M, Balbin R, Bozzano R, Nardelli BB, Cardin V, Casas B. 2019. Challenges for sustained observing and forecasting systems in the Mediterranean Sea. Front Mar Sci. 6:568. doi:10.3389/fmars.2019.00568.

Tolman HL. 1991. A third-generation model for wind waves on slowly varying, unsteady and inhomogeneous depths and currents. J Phys Oceanogr. 21:782–797. doi:10.1175/1520-0485(1991)021<0782:ATGMFW>2.0.CO;2.

Tolman HL. 2002. Alleviating the garden sprinkler effect in wind wave models. Ocean Mod. 4:269–289. doi:10.1016/S1463-5003(02)00004-5.

Tolman HL. 2008. A mosaic approach to wind wave modeling. Ocean Mod. 25:35–47. doi:10.1016/j.ocemod.2008.06.005.

Toomey T, Amores A, Marcos M, Orfila A, Romero R. 2022. Coastal hazards of tropical-like cyclones over the Mediterranean Sea. Journal of Geophysical Research: Oceans. 127(2):e2021JC017964. doi:10.1029/2021JC017964.

Tzioga I, Moriki A. 2023. Microplastic particles in Sandy Beaches of Thessaloniki Gulf, Greece. WSEAS Trans Environ Dev. 19:1380–1385. doi:10.37394/232015.2023.19.124.

Volpe G, Buongiorno Nardelli B, Colella S, Pisano A, Santoleri R. 2018. An operational interpolated ocean colour product in the Mediterranean Sea. In: Chassignet EP, Pascual A, Tintorè J, Verron J, editors. New frontiers in operational oceanography (GODAE OceanView). p. 227–244.

Wang H, Chen Q, Hu K, La Peyre MK. 2017. A modeling study of the impacts of Mississippi River diversion and sea-level rise on water quality of a deltaic estuary.

Estuaries Coasts. 40:1028–1054. doi:10.1007/s12237-016-0197-7.

Wang W, Bruyère C, Duda M, Dudhia J, Gill D, Kavulich M, Keene K, Lin H-C, Michalakes J, Rizvi S, et al. 2014. ARW version 3 modeling system user's guide. NCAR-MMM pp. 413. [accessed 2024 April 19]. https://www2.mmm.ucar.edu/wrf/users/docs/user_guide_V3/user_guide_V3.5/ARWUsersGuideV3.pdf.

WRF METEO AUTH. 2024. [accessed 2024 June 19]. https://meteo3.geo.auth.gr/WRF/home.html.

Zafirakou A. 2019. Oil Spill Dispersion Forecasting Models. Monitoring of Marine Pollution. IntechOpen. doi:10.5772/intechopen.81764.

Zervakis V, Krasakopoulou E, Tragou E, Kolovoyiannis V, Mamoutos I, Potiris M, Androulidakis I, Mosiou K, Ignatia Kalatzi M, Mazioti AA, Chatzilaou C. 2023. Development of a Coastal Oceanographic Observatory for the North Aegean Sea: The AEGIS projects. In EGU General Assembly Conference Abstracts (pp. EGU-13065).

Zgouridou A, Tripidaki E, Giantsis IA, Theodorou JA, Kalaitzidou M, Raitsos DE, Lattos A, Mavropoulou AM, Sofianos S, Karagiannis D, Chaligiannis I. 2022. The current situation and potential effects of climate change on the microbial load of marine bivalves of the Greek coastlines: An integrative review. Environ Microbiol. 24(3):1012–1034. doi:10.1111/1462-2920.15765.

Zodiatis G, Lardner R, Georgiou G, Demirov E, Pinardi N. 2003. Cyprus coastal ocean forecasting and observing system. In Elsevier Oceanography Series (Vol. 69, pp. 36–45). Elsevier.

Appendices

Appendix I: Additional comparisons with observations

Due to the lack of wave-buoy observations inside the Thermaikos Gulf (TG) basin, the WaveWatch-III's (WW-III) Hs time-series outputs have been validated against respective satellite (Jason-2/Phase-A) data (when available) for the entire year 2013–2014 (Krestenitis et al. 2014; Krestenitis et al. 2015) (Figure A1). The model's setup verification approach included a spatiotemporal collocation technique for the satellite observations and model results in hindcast and forecast mode, producing a fairly good agreement between observed and modelled wave heights, i.e. a Pearson product-moment correlation of $R_p > 0.72$ with $p_{value} < 0.01$, based on the Mann-Kendall (MK) correlation test (Mann 1945; Kendall 1975; i.e. at least 1% significance or 99% confidence level), a Root Mean Square Error of RMSE < 0.3 m and the normalised RMSE to observed Hs maxima (Hs,max,obs≈4 m) of RMSE/$H_{s,max,obs}$ = 7.5%. The correlation fit line between the two timeseries is $y = 0.95x$. Therefore, the operational wave simulations are considered to provide quite reliable estimations of the spectral wave characteristics for mixed sea conditions in the TG basin.

The simulated freshwater outflows in the TG, derived from the HEC-HMS simulations (Section 2.2), were evaluated against available flow rates, estimated through a stage-discharge curve and in situ measured stage data for the period of 2018 to 2020 (Figure A2). The observations were provided by the Soil and Water Resources Institute (SWRI 2024) near the estuary of Aliakmonas (Niseli station; Figure 1b). The Pearson correlation coefficient was 0.78 ($p_{value} <$ 0.001), while the RMSE was approximately 23 m^3/sec and the normalised RMSE was less than 10%, confirming the good performance of HEC-HMS to estimate the river outflow variability. It is noted that although the model performance statistics are very good, the model clearly tends to underestimate peak discharge situations. Two possible explanations are: (a) The model is highly dependent on the estimation of the discharge of the reservoirs located on the main stem of Aliakmon River. The total discharge of the dam, which is close to the estuaries, is not known but is estimated through the amount of energy produced (Section 2.2), and water release through its spillways cannot be incorporates in the model. (b) The stage–discharge curve used by the Niseli station operators may overestimate the flow rate for high water levels.
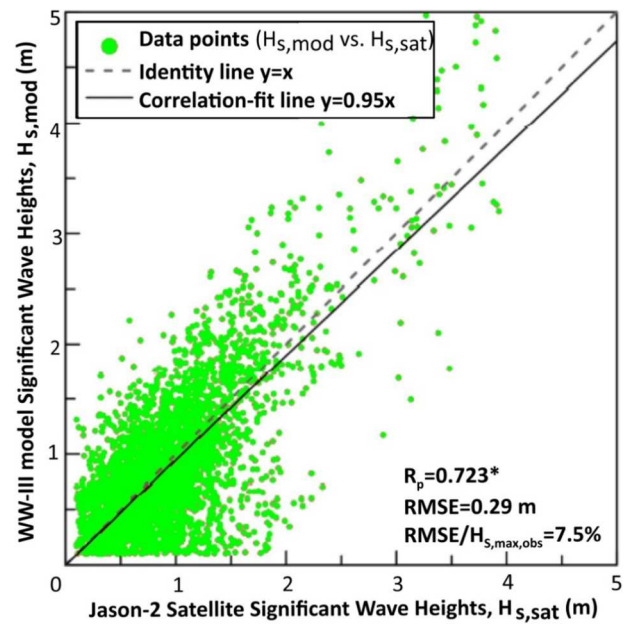
Figure A1. Scatter Plot of modelled vs. satellite Significant Wave Heights ($H_{s,mod}$ vs. $H_{s,sat}$) derived by WaveWatch-III (WW-III) simulations and Jason-2 (L3 product). The correlation-fit line, the Pearson correlation coefficient R_P (*statistically significant value), the Root Mean Square Error (RMSE), and the normalised RMSE (%) are shown.
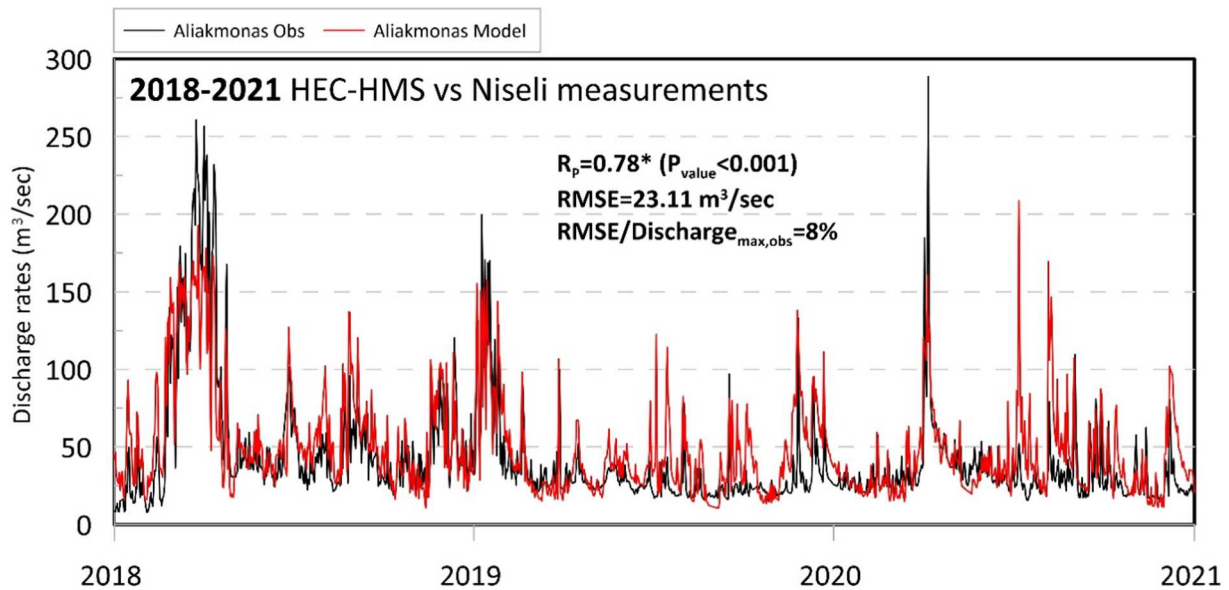
Figure A2. Comparison between HEC-HMS simulated discharge rates (red line) and respective daily measurements (blue lines) at Niseli station (Aliakmonas; Figure 1c) from 2018 to 2020. The Pearson correlation (R_P), the p_{value} of the correlation significance test (*statistically significant value), the Root Mean Square Error (RMSE), and the normalised RMSE with the maximum observed discharge rate are also shown.